TM6. The phenoxy-benzoic acid group of AK317 interacts with S180 and K191. S180 is a part of ECL2, whereas K191 in TM5 is likely located above the plane of the extracellular region. The pyrazol group of AK530, on the other hand, bends towards the cytoplasmic region and makes the inhibitor bind deeper into the cavity. There are no direct interactions of AK530 with K191, but it seems to be forming a favorable conformation of the binding pocket by an intramolecular hydrogen bond network with G163 and T195 (Fig. 5c). K191, located in the upper domain of TM5, can be considered to be an extracellular residue as well, since a part of K191 is located above the cellular plane (Fig. 2). We speculate that the direct interactions of AK317 with the ECL2 residues such as S180 and with the residues in the extracellular region (such as K191) are responsible for its high antiviral IC_{50} of 2 nM (Table 1). In spite of being a weaker binder compared to AK530, the interactions of the phenoxy-benzoic acid group of AK317 seem to be responsible for its comparable antiviral potency with AK530, which has no direct interaction with ECL2 residues in the vicinity of TM4 and TM5.

The binding cavities of both AK530 and AK317 are mostly lipophilic (Fig. 4a and b). The only strongly hydrophilic regions are towards the extracellular loop region. The shape and volume of the cavities are slightly different for these two inhibitors, as CCR5 is likely to undergo conformational changes to different extents to accommodate these two inhibitors. The unoccupied regions of the cavity suggest new optimization ideas for these inhibitors. For example, substituents of AK530 that can potentially interact with K191 may increase its antiviral potency even further.

Determination of interatomic distances between key amino acids when AK317 and AK530 bind to CCR5

In an attempt to examine whether the binding of AK317 or AK530 to CCR5 causes significant changes in interatomic distances between key amino acids that form the hydrogen bond network seen in the unbound CCR5 as described above (Fig. 3), we carried out molecular dynamics simulation for 4800 ps for AK317- and AK530-bound CCR5, and analyzed critical interatomic distances with the unbound conformation (Fig. 7a–c). In the unbound conformation, Y108 in TM3 was in close proximity to Y251 located in TM6 and had a hydrogen bond interaction with E283 in TM7 (Figs. 3 and 7a and b). In the AK317-bound CCR5, Y108 had rotated away from Y251, and the hydrogen bond interaction between Y108 and E283 was lost. Rotation of Y108 away from Y251 and disruption of hydrogen bond interaction between Y108 and E283 were also observed when AK530 bound to CCR5. TM2 and TM3 can be thought to be in a single plane (above the plane of the paper), and TM6 and TM7 can be thought to be in a different plane (behind the plane of the paper). The rearrangement of Y108 was necessary for the formation of the binding cavity between the transmembrane helices for inhibitor binding. Furthermore, in the unbound CCR5 structure, E283 is hydrogen-bonded to S180, which is part of the ECL2 (Fig. 3). In fact, E283 moved considerably away from S180 in the inhibitor-bound models of CCR5 (Figs. 5c, 6b, and 7c). Disruption of hydrogen bonds between transmembrane residues and a network of hydrogen bonds mediated through water molecules are known to give rise to the change in the intracellular loop conformation of bovine rhodopsin.[29,30] Change in ionic interactions between transmembrane residues is also thought to be responsible for the activation of β_2-adrenergic receptor.[34] We speculate that the rotation of Y108 away from the vicinity of Y251, the loss of hydrogen bond interaction between Y108 and E283, and the loss of hydrogen bond interaction between E283 and S180 presumably change the conformation of the ECL2 that is crucial for the binding of the gp120/CD4 complex. These models of unbound and inhibitor-bound CCR5 may give further insights into the mechanism of the inhibition of CCR5 inhibitors involving transmembrane and extracellular residues interacting with each other.

Structural changes in ECL2 caused by CCR5 inhibitors block the binding of CCR5-specific monoclonal antibodies to CCR5

Our structural analyses described above demonstrated that AK530 relatively well maintained its CCR5 binding with the K191A substitution, while AK317 significantly reduced its interactions with $CCR5_{K191A}$, prompting us to examine whether the different CCR5-binding profiles of these two inhibitors led to different dynamics in their interactions with CCR5-specific monoclonal antibodies (mAbs). To this end, we examined whether AK530 and AK317 blocked the binding to CCR5 expressed on CHO cells of four mAbs: 45531 [specific for the C-terminal half of ECL2 (ECL2B)], 45523 (reactive to CCR5 multidomain), 2D7 [specific for the N-terminus of ECL2 (ECL2A)], and 45549 (reactive to CCR5 multidomain).[25,35,36] In this mAb-binding blocking assay, the cells were incubated with each inhibitor for 30 min, followed by the addition of a mAb. As shown in Fig. 8, AK317 effectively inhibited the binding of mAb 45531 with an IC_{50} value of 16.3 nM, while the inhibition by AK530 was much less, with an IC_{50} value of 746 nM. AK317 also blocked the binding of mAb 45523 with an IC_{50} value of 282 nM, while AK530 did so with an IC_{50} value of >1 μM. None of the inhibitors blocked the binding of mAb 2D7 or 45549. When the cells were first exposed to a mAb, followed by the addition of each inhibitor, the resultant inhibition levels were virtually the same (data not shown). Considering that these CCR5 inhibitors are lodged in a hydrophobic pocket at the interface of ECL2 and the upper transmembrane domain (Figs. 4–6), the observed inhibition of mAb binding by CCR5 inhibitors presumably occurred through the allosteric changes secondarily caused by CCR5 binding of the inhibitor, but not through their competition over binding to the antigenic epitope (s) of CCR5.

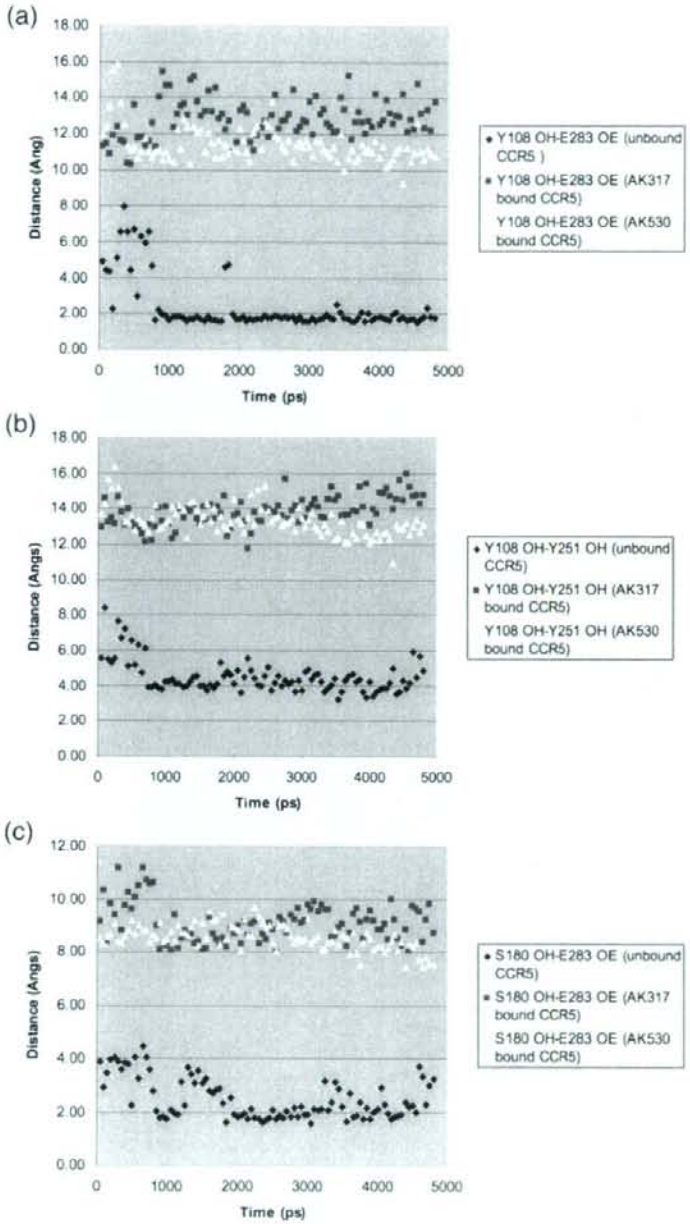

Fig. 7. Key interatomic distances from molecular dynamics simulation of AK317-bound, AK530-bound, and unbound CCR5. Molecular dynamics simulation for AK317- and AK530-bound CCR5 was conducted for 4800 ps, and critical interatomic distances between key amino acids were determined. A hydrogen bond is present if the interatomic distance is <3 Å. (a) Distance between Y108 (hydroxyl hydrogen, PDB atom-type OH) and E283 (carboxylate oxygen, PDB atom-type OE). In the unbound conformation, there is a strong hydrogen bond interaction between Y108 in TM3 and E283 in TM7. Y108 and E283 have to move away from each other to form the binding cavity for the inhibitor to bind, and there is no hydrogen bond between these residues after AK317 and AK530 binding. (b) Distance between Y108 and Y251 hydroxyl oxygen: the tyrosines have moved away from each other after inhibitor binding. (c) Distance between E283 (carboxylate oxygen, PDB atom-type OE) and S180 (hydroxyl hydrogen, PDB atom-type OH). In the unbound conformation, E283 in TM7 has hydrogen bond interactions with S180 in ECL2. This hydrogen bond is disrupted for AK317- and AK530-bound CCR5.

Effects of amino acid substitutions in CCR5 on HIV-1-gp120-elicited cell fusion

In order to better understand conformational changes arising in ECL2 and to determine amino acids that are critical for the cellular entry of HIV-1, we examined the effects of single and multiple amino acid substitutions in ECL2 on HIV-1-gp120-elicited cell fusion. Figure 9 shows the magnitude of cell–cell fusion between tat$^+$,env$^+$ 293T cells and Luc$^+$,CCR5$^+$ MAGI cells in the HIV-1-gp120-elicited cell–cell fusion assay. Seven single amino acid substitutions introduced into CCR5 resulted in a substantial reduction (>70%) in the HIV-1-envelope-protein-elicited fusion level (Fig. 9). Three of these single amino acid substitutions (E172A, L174A, and C178A) are located in the ECL2 with an antiparallel β-hairpin structure, while C101A and G163R are in TM3 and TM4, respectively,

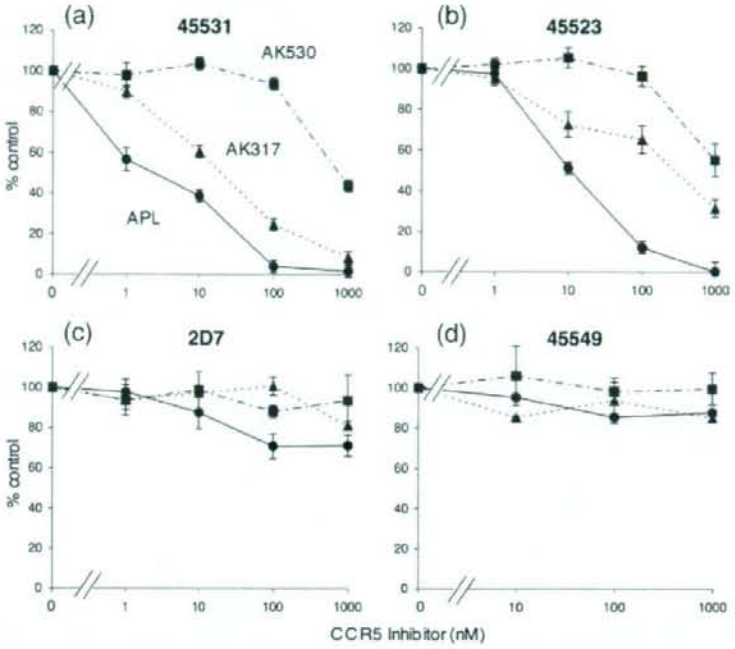

Fig. 8. Inhibition of the binding of anti-CCR5 mAbs by AK530, AK317, and APL. Inhibition by three CCR5 inhibitors of the binding of anti-CCR5 mAbs [45531 (a), 45523 (b), 2D7 (c), and 45549 (d)], which recognize the extracellular domain (s) of CCR5, is illustrated. CCR5-overexpressing CHO cells were incubated with each of the fluorescein-isothiocyanate-conjugated anti-CCR5 mAbs in the presence of various concentrations of a CCR5 inhibitor, and fluorescence intensity on the cells was determined. Each value was compared to that obtained without an inhibitor and is shown as percent control.

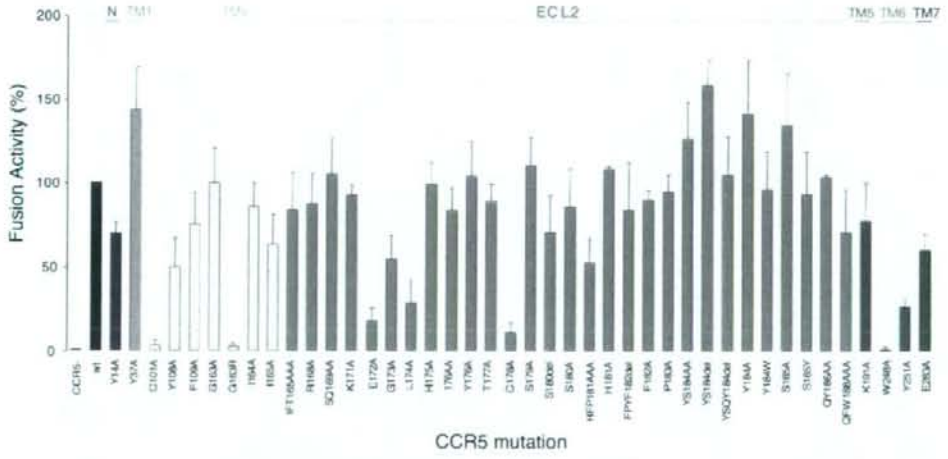

Fig. 9. Effects of amino acid substitution(s) and deletion(s) on HIV-1-gp120-elicited cell–cell fusion. $CD4^+$ MAGI cells that expressed sufficient numbers of wild-type or mutated CCR5 were cultured with HIV-1 env^+, tat^+ 293T cells for 6 h, and fusion efficiency was determined with luciferase activity (luminescence levels) using the reporter gene activation assay. The magnitude of luminescence levels with mutant CCR5 is expressed as percent fusion (percent control compared to the luminescence level with wild-type CCR5). Note that three single amino acid substitutions (E172A, L174A, and C178A), which resulted in a substantial reduction in the fusion level (>70%), are located in the ECL2 that has an antiparallel β-hairpin structure (Figs. 2 and 3), while C101A and G163R are in TM3 and TM4, respectively, and W248A and Y251A are in TM6.

and W248A and Y251A are in TM6 (Figs. 2 and 3). Note that E172 is at the NH_2 end of the β-sheet structure of ECL2 and that C178 also belongs to the β-hairpin structural motif (Fig. 2). This finding strongly suggests that these mutations led to the disruption of ECL2's β-sheet structure and resulted in a significant reduction in the cell–cell fusion. Thus, the β-sheet structure of ECL2 seems to be critical for the cellular entry of HIV-1. It is noteworthy that although the two amino acids E172 and L174 do not interact with CCR5 inhibitors (Figs. 4–6), their mutations significantly reduced cell–cell fusion (Fig. 9).

The C101A and C178A substitutions are thought to disrupt the disulfide bond between C101 and C178, which is crucial for the maintenance of the robust ECL2 structure, as demonstrated in this study. Thus, both C101A and C178A substitutions probably led to the aborted HIV-1-envelope-elicited fusion. G163, located in TM4, does not interact directly with AK530, AK317, or APL, but is responsible for maintaining the shape of the binding cavity by its hydrogen bond interactions with S180, K191, and T195 (Figs. 5 and 6). G163R substitution also resulted in virtually a complete loss of fusion (Fig. 9). This is consistent with earlier observations that G163R mutation results in the loss of HIV-1 infectivity.[22,31]

Amino acids within ECL2 at positions 179 through 190 appeared not to have a crucial role in the HIV-1-envelope-elicited fusion. Indeed, the amino acid substitutions in these positions did not significantly reduce the fusion (Fig. 9). It is noteworthy that these amino acids are located distant from the binding cavity for CCR5 inhibitors (Figs. 2, 5, and 6). It is also of note that W248 has hydrogen bond interactions with Y251 and is thought to play a role in maintaining the conformation of ECL2 (Fig. 3), explaining the reason that W248A substitution results in loss of fusion.

Interestingly, both C178A and C101A substitutions substantially reduced CCR5 binding of the three CCR5 inhibitors (AK530, AK317, and APL), but not that of SCH-C or TAK-779.[22] In particular, APL forms hydrogen bonds with C178 and, additionally, has tight interactions with the intramolecular hydrogen bond network (S180/G163/K191/T195).[22] AK317 also has interactions with the S180/G163/K191/T195 network (Fig. 6). Thus, SDP-containing CCR5 inhibitors, especially APL and AK317, appear to have greater interactions with ECL2 compared to other non-SDP-containing CCR5 inhibitors such as SCH-C or TAK-779. Our observation that AK530 has the greatest binding affinity for CCR5 (Table 1) but exerts less potent anti-HIV-1 activity (Table 1) may be related to its reduced interactions with ECL2 (Figs. 5 and 7). Such tight interactions with ECL2 may represent a feature conferring potent anti-HIV-1 activity on CCR5 inhibitors, different from allosteric changes caused by CCR5 inhibitors.

Discussion

In the present study, we demonstrated that two novel CCR5 inhibitors, AK530 and AK317, are lodged in a hydrophobic cavity located between the upper transmembrane domain and ECL2. CCR5 is a member of GPCRs, the largest superfamily of proteins in the body. Understanding the structure of human GPCRs would be invaluable in elucidating their roles in a number of biological processes and should also greatly aid in designing therapeutics. In particular, the elucidation of the detailed structure of human CCR5 and its interactions with HIV-1 envelope glycoprotein should help establish a strategy for HIV-1 intervention. However, no crystal structures of human CCR5 are yet available; bovine rhodopsin and β_2-adrenergic receptors are the only GPCR species for which crystallographic data have been obtained.[32,37] Thus, we have previously explored an alternate approach: combination of site-directed-mutagenesis-based saturation binding assay and molecular modeling based on the crystallographic data of bovine rhodopsin.[22] The site-directed-mutagenesis-based saturation binding assay alone can give certain insights as to which residues of the receptor are implicated in the binding with the inhibitor. However, it does not indicate which specific atoms of the residue are involved. Homology modeling and docking give insights to interactions between atoms, but these methods produce multiple possible solutions, and it is difficult to differentiate between distinct interactions that are within a small energy range. Combining these complementary methods of site-directed mutagenesis and computational protein structure determination has made it possible to conduct robust structural analyses.[22] However, certain validation of the model is crucial. Thus, in the present study, we chose five amino acid residues of CCR5 that were judged to be critical for APL binding based on our previous analysis, and additional mutagenesis studies were carried out. When an amino acid substitution (P84H, C101A, F109A, T195P, or T195S) was introduced into $CCR5_{WT}$ and saturation binding assay was performed using [^{3}H]APL, all K_d values proved to be >100 nM, while the K_d value of [^{3}H]APL with wild-type CCR5 was 3.6 nM. This corroborated the notion that we previously made[22]—that the alternate approach using saturation binding assay, combined with our computational protein structure determination, can provide reasonably robust structural insights.

In the present study, we attempted to obtain a refined structural CCR5 model through molecular dynamics computation. In an unbound CCR5, we identified key interactions between residues located in different transmembranes, and between transmembrane and ECL2 amino acid residues. Amino acids involved in such intramolecular interactions included Y37, H175, Y108, Y251, E283, and S180. The intramolecular hydrogen bond interactions observed among different transmembrane regions, and between transmembrane and ECL2 loop presumably stabilize the unbound conformation of CCR5 (Fig. 3). In order to determine the structures of AK317, and AK530 complexed to CCR5, we utilized a novel algorithm to incorporate receptor flexibility and induced-fit effects.[38] The optimized AK317–CCR5 and AK530–CCR5 complex structures indica-

ted a rotation of Y108(TM3) away from both Y251 (TM6) and E283(TM7) to make room for the inhibitor within the transmembrane helices. As a result of inhibitor binding, the hydrogen bond between Y108 and E283 and that between E283 and S180 seen in the unliganded CCR5 were disrupted, and these residues formed hydrogen bond or tight van der Waals interactions with the inhibitors instead (Figs. 5–7). The disruption of interhelix residue interactions may cause movement of the transmembrane helices and changes in the conformation of ECL2. A similar mechanism, involving disruption of interhelix hydrogen bond interactions, is thought to be responsible for changes in loop conformation in rhodopsin[27,29] and in the activation of β_2-adrenergic receptor.[34] Note that Y37(TM1) is involved in a hydrogen bond interaction with ECL2 via H175. We have observed that Y37 interacts with SCH-C and TAK-779.[22] These arrangements of hydrogen bond interactions between transmembrane helices and ECL2 should also provide an explanation of the reason that these inhibitors exert potent antiviral activity against HIV-1. Thus, the disruption of hydrogen bond interactions between transmembrane helices, and between transmembrane helices and ECL2, should be a mechanism of allosteric inhibition observed by the binding of CCR5 inhibitors to a binding domain residing mostly within the transmembrane residues.

We also examined the interplays of ECL2 and selected amino acid residues that consist of the largest hydrophobic cavity within CCR5, which accommodate small-molecule CCR5 inhibitors. Our previously published data[22] and data by others[19,23] showed that two CCR5 inhibitors (SCH-C and TAK-779) have no direct interactions with amino acid residues in the extracellular domain, including ECL2. However, all the three SDP-based CCR5 inhibitors that we examined (AK530, AK317, and APL) had substantial interactions with amino acids in ECL2, in particular with C178, which is located in the antiparallel β-hairpin structural motif of ECL2, and with K191, which is located at the interface of ECL2 and TM5 (Figs. 4–6). The C178A substitution virtually abrogated the binding of the three inhibitors to CCR5. C178 is presumed to form a disulfide bond with C101 of TM3 and seems to be critical for the conformation of ECL2. The disruption of the disulfide bond with C178A mutation may result in decreased binding of the three SDP-based inhibitors. Our previous observation[22] and the report from others[19,23] that the same C178A substitution did not affect the CCR5 binding of two other CCR5 inhibitors, SCH-C and TAK-779, suggest that C178 plays a unique but critical role in the binding of AK530, AK317, and APL. In the present study, K191A substitution also virtually nullified the CCR5 binding of AK317 and APL (Table 2), although it did not significantly affect the binding of AK530 probably due to the absence of hydrogen bonding between AK530 and K191 (Fig. 5). Taken together, these data suggest that, unlike the cases of SCH-C and TAK-779, at least a part of the hydrophobic cavity where AK530, AK317, and APL are lodged within CCR5 involves ECL2. The disruption of ECL2's β-sheet structure by the removal of disulfide bond through C101A and C178A substitutions virtually nullified both the binding of all three CCR5 inhibitors and the HIV-1-gp120-elicited fusion. This strongly suggests that ECL2 plays a crucial role not only in the binding of the three CCR5 inhibitors but also in the interaction of HIV-1 envelope glycoproteins with CCR5. The data also suggest that at least two amino acids in ECL2, C178 and K191, can be potential targets for the design of CCR5 inhibitors.

Several studies have shown that the resistance against a CCR5 inhibitor emerged without the change in coreceptor usage.[39–44] Resistant R5-HIV-1 variants were reportedly obtained by passage 22 for AD101,[40] passage 43 for TAK-652,[41] passage 20 for VVC,[43] and passages 12–18 for MVC.[42] However, we have failed in selecting R5-HIV-1 variants resistant to APL even after 60 passages *in vitro* (over ~1.5 years) (Nakata *et al.*, unpublished data), although the possibility of the emergence of HIV-1 variants resistant to APL cannot be ruled out in other settings.[45] Pugach *et al.* demonstrated that one of the mechanisms by which HIV-1 becomes resistant to CCR5 inhibitors such as VVC is by "noncompetitive resistance"—a process in which a resistant virus continues to enter target cells regardless of the concentration of the inhibitor once HIV-1 has acquired the ability to use the inhibitor-bound CCR5 for entry.[44] Of note, Westby *et al.* reported that a virus resistant to MVC retained susceptibility to APL, suggesting that the virus can use MVC-bound CCR5 for entry, but cannot use APL-bound CCR5.[42] Thus, APL is likely to have such a profile that does not allow or delay HIV-1 acquisition of the ability to utilize the "APL-bound" CCR5 for its cellular entry. This potentially favorable property of APL may be related to the direct interactions of APL with amino acids in ECL2, producing "substantially distorted" ECL2 with which HIV-1 gp120 cannot get engaged for its cellular entry, while certain unique allosteric changes in ECL2 conformation following the binding of APL might also explain the substantial delay or lack of the emergence of APL-resistant HIV-1.

The present data, taken together, demonstrate that structural modeling analysis, coupled with CCR5-binding affinity data, should help understand the structural/molecular mechanism of the inhibition of HIV-1 infection by CCR5 inhibitors. The data should not only help delineate the structural dynamics of CCR5 following ligand binding but also aid in the design of therapeutic inhibitors. The data, in particular, demonstrate that by studying the properties of unbound and inhibitor-bound CCR5, transmembrane residues such as Y108, Y251, and E283 are important for gp120 fusion, HIV infectivity,[22] and inhibitor binding. The loss of hydrogen bond interactions among these key transmembrane residues and the interactions between E283 and S180, which are essential for the formation and maintenance of the binding pocket for CCR5 inhibitors, might be responsible for changes in ECL2 conformation, providing insights into the mechanism of gp120 inhibition.

Materials and Methods

Reagents

Three SDP derivatives, APL,[14,46] AK530, and AK317, are discussed in the present report. The methods for the synthesis and physicochemical profiles of AK530 and AK317 will be described elsewhere. Tritiation of these three CCR5 inhibitors was conducted as previously reported.[14] The structures of these three CCR5 inhibitors are illustrated in Fig. 1.

Cells, viruses, and anti-HIV-1 assay

CHO cells expressing wild-type CCR5 ($CCR5_{WT}$-CHO cells) or mutant CCR5 ($CCR5_{MT}$-CHO cells)[22] were maintained in Ham's F-12 medium (Invitrogen, Carlsbad, CA), supplemented with 10% fetal calf serum (FCS; HyClone, Logan, UT) in the presence of 100 μg/ml zeomycin (Invitrogen). The MAGI cell line[47] was provided by the National Institutes of Health (NIH) AIDS Research and Reference Reagent Program and cultured in Dulbecco's modified Eagle's medium (DMEM) supplemented with 10% FCS, 200 μg/ml G418, and 100 μg/ml hygromycin B. MAGI-CCR5 cells[48] were maintained in DMEM supplemented with 10% FCS, 200 μg/ml G418, 100 μg/ml hygromycin B, and 100 μg/ml zeomycin. 293T cells were cultured in DMEM with 10% FCS. PBM cells were isolated from buffy coats of HIV-1-seronegative individuals and activated with 10 μg/ml PHA prior to use, as previously described.[8] Two wild-type R5-HIV-1 strains were employed for drug susceptibility assays: $HIV\text{-}1_{Ba\text{-}L}$[49] and $HIV\text{-}1_{JRFL}$.[50] Antiviral assays using PHA-PBM (p24 assay) and MAGI assay using MAGI-CCR5 cells were also conducted as previously reported.[8]

Fluorescence-activated cell sorter analysis and mAb displacement assay

$CCR5_{WT}$-CHO cells (2×10^5) were exposed to differing concentrations (1 nM–1 μM) of a CCR5 inhibitor for 30 min, followed by the addition of a fluorescein-isothiocyanate-conjugated anti-CCR5 mAb, 2D7 (BD PharMingen, San Diego, CA), 45523, 45531, or 45549 (R&D Systems, Minneapolis, MN), and further incubated for 30 min at 4 °C. Cells were washed and analyzed on an flow cytometer (FACSCalibur; BD Biosciences, San Jose, CA). Each fluorescent activity in the presence of a drug was compared to that obtained in the absence of inhibitors and shown as percent control.

Saturation binding assay

A panel of mutant CCR5-expressing CHO cells[22] was used for saturation binding assays. The CHO cell lines expressing mutant CCR5 P84H ($CCR5_{P84H}$-CHO cells), C101A, L104D, F109A, T195A, T195P, T195S, and W248A were newly generated and used. The saturation binding assay using tritiated CCR5 inhibitors ([^{3}H]APL, [^{3}H]AK530, and [^{3}H]AK317) and wild-type or mutant CCR5-expressing CHO cells was conducted as previously described.[14] In brief, wild-type or mutant $CCR5^+$ CHO cells (1.5×10^5 cells/well) were plated onto 48-well flat-bottomed culture plates, incubated for 24 h, exposed to various concentrations of each [^{3}H]CCR5 inhibitor, washed thoroughly, and lysed with 0.5 ml of 1 N NaOH, and radioactivity in the lysates was measured. The K_d (dissociation) values of CCR5 inhibitors and the maximal binding values (B_{max} = number of CCR5 per cell) were calculated based on their specific radioactivity using GRAPHPAD PRISM software (Intuitive Software for Science, San Diego, CA).

CCR5 homology model

A homology model of CCR5 was built as follows. The sequence of CCR5 (352 amino acids) was aligned against the sequence of bovine rhodopsin (348 amino acids). The recently determined crystal structure of bovine rhodopsin by Okada *et al.* was used as the template structure [Protein Data Bank (PDB) accession ID 1U19].[27] The alignment was manually adjusted to ensure that the conserved GPCR residues were aligned as follows: in TM1, N55 of bovine rhodopsin was aligned to N48 of CCR5; in TM2, D83 was aligned to D76; in TM3, E134-R135-Y136 was aligned to D125-R126-Y127; in TM4, W161 was aligned to W153; in TM5, P215 was aligned to P206; in TM6, W265-x266-P267-Y268 was aligned to W248-x249-P250-Y251; in TM7, P303 was aligned to P294; in H8, F313 was aligned to F304. Secondary structure prediction assigned the length of each helix, β-sheet, and loop segment. After building the transmembrane helices, the loops connecting the different transmembrane domains were built using the ultraextended sampling protocol in Prime (Prime, version 1.6, 2007; Schrödinger, LLC, New York, NY), which does a more exhaustive sampling of the loop conformations.[51] The side chains were predicted using the rotamer library of Xiang and Honig.[52] The structure was minimized in implicit water with the OPLS2005 force field,[53] as implemented in MacroModel (MacroModel 9.1, 2005; Schrödinger, LLC).

All atom molecular dynamics simulations, without using any nonbonded cutoff distances, were carried out on CCR5. A constant temperature of 300 K and SHAKE constraints for hydrogen bonds were used. The GB/SA continuum solvation model, with water as the solvent, was used.[54] Using a time step of 1 fs, the structures were equilibrated for 100 ps. The simulation was carried out for 4800 ps on a Linux cluster, and structures were monitored at 50-ps intervals.

Structural modeling of the interactions of CCR5 inhibitors with CCR5

After building the initial model of CCR5, the CCR5–inhibitor complex structures were further defined with an iterative optimization of CCR5 and ligand structures in the presence of each other, using software tools from Schrödinger, LLC, as described below. The conformational flexibilities of both CCR5 and CCR5 inhibitors were taken into account. The molecular structures of AK530, AK317, and APL were obtained by minimization using the MMFF94 force field, as implemented in MacroModel. For each minimized inhibitor configuration, a set of low-energy structures was generated by performing a Monte Carlo sampling of their conformations. Thus, obtained structures were used as starting structures for docking calculations where their conformations were further refined.

The protonation states of CCR5 residues were assigned, and residues more than 20 Å from the active site were neutralized. We initially failed to obtain energetically favorable inhibitor–CCR5 complex structures by using a *rigid* CCR5 structure because of the unfavorable steric interaction of the side chains of the active site residues with the inhibitors. In an attempt to place an inhibitor within CCR5, after analysis of the steric clashes, the active site

was artificially enlarged by mutating Y108, C178, E283, and M287 to Ala. The van der Waals radii of inhibitor atoms were scaled by a factor of 0.70 to reduce steric clashes and docked into CCR5. After obtaining an initial "guess" set of CCR5–inhibitor complexes, residues 108, 178, 283, and 287 were mutated back from Ala to their original states. CCR5 atoms within 15 Å of an initially placed inhibitor were subsequently refined. It was achieved by using the rotamer library of Xiang and Honig and by optimizing each side chain one at a time, holding all other side chains fixed.[52] After convergence, all side chains were simultaneously energy-minimized to remove any remaining clashes. The inhibitors were docked again and scored to estimate their relative affinity. The extraprecision mode of Glide,[55,56] which penalized unfavorable and unphysical interactions, was used. The docked complexes with higher scores were visually examined along with the mutational data to select the best possible CCR5–inhibitor complex.

Visualization, structural refinement, and docking were performed using Maestro 7.5, MacroModel 9.1, Prime 1.6, Glide 4.5, and IFD script[38] from Schrödinger, LLC (2007). Computations were carried out on a multiprocessor SGI Origin 3400 computer platform and on a Beowulf-type Linux cluster.

HIV-1-gp120-elicited cell–cell fusion assay

The entire human *CCR5* gene, including a stop codon, was amplified using pZeoSV-*CCR5*[48] as template. The polymerase chain reaction product was ligated into pcDNA6.2/cLumio-DEST vector (Invitrogen), cloned in accordance with the manufacturer's recommendation, and termed pcDNA6.2-$CCR5_{WT}$ (a CCR5 expression vector). A variety of plasmids carrying a mutant *CCR5*-encoding gene (pcDNA6.2-$CCR5_{MT}$) were subsequently generated by employing the site-directed mutagenesis technique. An HIV-1 *tat* expression vector (pcDNA6.2-HIV-*tat*) was also generated using the same method. For the generation of HIV-1-gp120-overexpressing 293T cells, an HIV envelope expression vector, pCXN-JR*env*,[48] was employed. A reporter (luciferase) gene containing plasmid pLTR-*Luc*E[57] was provided by the NIH AIDS Research and Reference Reagent Program. The envelope expression vector and tat expression vector (0.5 μg each) were cotransfected into 293T cells (2×10^5; 3 ml in six-well microculture plates) using Lipofectamine 2000 (Invitrogen), while the $CCR5_{WT}$ or mutant CCR5 expression vector and pLTR-*Luc*E (0.5 μg each) were cotransfected into MAGI cells (2×10^5; 3 ml in six-well microculture plates). On the next day, both the cotransfected cells were harvested and mixed in a well of 96-well plates (2×10^4 cells each). The cotransfected cells were incubated further for 6 h, the luciferase activity in each well was detected using Bright-Glo Luciferase Assay System (Promega, Madison, WI), and its luminescence level was measured using Veritas Microplate Luminometer (Turner BioSystmes, Sunnyvale, CA). Nonspecific luciferase activity was determined with the luminescence level in the well containing control tat^+,env^- 293T cells and Luc^+,$CCR5^+$ MAGI cells, and the value of the nonspecific luminescence level was subtracted from each experimental luminescence level.

Protein Model DataBase accession code

The coordinates for the models of ligand-free CCR5, CCR5–AK317, and CCR5–AK530 complexes with accession codes PM0075224, PM0075223, and PM0075221, respectively, have been deposited in the Protein Model DataBase†.

Acknowledgements

The authors thank David A. Davis and Yasuhiro Koh for critical reading of the manuscript. This work was supported, in part, by the Intramural Research Program of the Center for Cancer Research, National Cancer Institute, NIH, and in part by a Grant for the Promotion of AIDS Research from the Ministry of Health, Welfare, and Labor of Japan, and the Grant to the Cooperative Research Project on Clinical and Epidemiological Studies of Emerging and Reemerging Infectious Diseases (Renkei Jigyo: No. 78, Kumamoto University) of Monbu-Kagakusho (H. M.). We also thank the Center for Information Technology, NIH, for providing computational resources on the NIH Beowulf Linux cluster, and Susan Chacko and David Hoover for help with batch job configuration on the cluster.

References

1. Raport, C. J., Gosling, J., Schweickart, V. L., Gray, P. W. & Charo, I. F. (1996). Molecular cloning and functional characterization of a novel human CC chemokine receptor (CCR5) for RANTES, MIP-1beta, and MIP-1alpha. *J. Biol. Chem.* **271**, 17161–17166.
2. Alkhatib, G., Combadiere, C., Broder, C. C., Feng, Y., Kennedy, P. E., Murphy, P. M. & Berger, E. A. (1996). CC CKR5: a RANTES, MIP-1alpha, MIP-1beta receptor as a fusion cofactor for macrophage-tropic HIV-1. *Science*, **272**, 1955–1958.
3. Wu, L., Gerard, N. P., Wyatt, R., Choe, H., Parolin, C., Ruffing, N. *et al.* (1996). CD4-induced interaction of primary HIV-1 gp120 glycoproteins with the chemokine receptor CCR-5. *Nature*, **384**, 179–183.
4. Trkola, A., Dragic, T., Arthos, J., Binley, J. M., Olson, W. C., Allaway, G. P. *et al.* (1996). CD4-dependent, antibody-sensitive interactions between HIV-1 and its co-receptor CCR-5. *Nature*, **384**, 184–187.
5. Deng, H., Liu, R., Ellmeier, W., Choe, S., Unutmaz, D., Burkhart, M. *et al.* (1996). Identification of a major co-receptor for primary isolates of HIV-1. *Nature*, **381**, 661–666.
6. Kilby, J. M. & Eron, J. J. (2003). Novel therapies based on mechanisms of HIV-1 cell entry. *N. Engl. J. Med.* **348**, 2228–2238.
7. Baba, M., Nishimura, O., Kanzaki, N., Okamoto, M., Sawada, H., Iizawa, Y. *et al.* (1999). A small-molecule, nonpeptide CCR5 antagonist with highly potent and selective anti-HIV-1 activity. *Proc. Natl Acad. Sci. USA*, **96**, 5698–5703.
8. Maeda, K., Yoshimura, K., Shibayama, S., Habashita, H., Tada, H., Sagawa, K. *et al.* (2001). Novel low molecular weight spirodiketopiperazine derivatives potently inhibit R5 HIV-1 infection through their antagonistic effects on CCR5. *J. Biol. Chem.* **276**, 35194–35200.

†http://mi.caspur.it/PMDB

9. Watson, C., Jenkinson, S., Kazmierski, W. & Kenakin, T. (2005). The CCR5 receptor-based mechanism of action of 873140, a potent allosteric noncompetitive HIV entry inhibitor. *Mol. Pharmacol.* **67**, 1268–1282.
10. Tagat, J. R., McCombie, S. W., Nazareno, D., Labroli, M. A., Xiao, Y., Steensma, R. W. *et al.* (2004). Piperazine-based CCR5 antagonists as HIV-1 inhibitors: IV. Discovery of 1-[(4,6-dimethyl-5-pyrimidinyl)carbonyl]-4-[4-[2-methoxy-1(*R*)-4-(trifluoromethyl)phenyl] ethyl-3(*S*)-methyl-1-piperaz inyl]-4-methylpiperidine (Sch-417690/Sch-D), a potent, highly selective, and orally bioavailable CCR5 antagonist. *J. Med. Chem.* **47**, 2405–2408.
11. Dorr, P., Westby, M., Dobbs, S., Griffin, P., Irvine, B., Macartney, M. *et al.* (2005). Maraviroc (UK-427,857), a potent, orally bioavailable, and selective small-molecule inhibitor of chemokine receptor CCR5 with broad-spectrum anti-human immunodeficiency virus type 1 activity. *Antimicrob. Agents Chemother.* **49**, 4721–4732.
12. Seto, M., Aikawa, K., Miyamoto, N., Aramaki, Y., Kanzaki, N., Takashima, K. *et al.* (2006). Highly potent and orally active CCR5 antagonists as anti-HIV-1 agents: synthesis and biological activities of 1-benzazocine derivatives containing a sulfoxide moiety. *J. Med. Chem.* **49**, 2037–2048.
13. Imamura, S., Ichikawa, T., Nishikawa, Y., Kanzaki, N., Takashima, K., Niwa, S. *et al.* (2006). Discovery of a piperidine-4-carboxamide CCR5 antagonist (TAK-220) with highly potent anti-HIV-1 activity. *J. Med. Chem.* **49**, 2784–2793.
14. Maeda, K., Nakata, H., Koh, Y., Miyakawa, T., Ogata, H., Takaoka, Y. *et al.* (2004). Spirodiketopiperazine-based CCR5 inhibitor which preserves CC-chemokine/CCR5 interactions and exerts potent activity against R5 human immunodeficiency virus type 1 *in vitro*. *J. Virol.* **78**, 8654–8662.
15. Fatkenheuer, G., Pozniak, A. L., Johnson, M. A., Plettenberg, A., Staszewski, S., Hoepelman, A. I. *et al.* (2005). Efficacy of short-term monotherapy with maraviroc, a new CCR5 antagonist, in patients infected with HIV-1. *Nat. Med.* **11**, 1170–1172.
16. Cormier, E. G. & Dragic, T. (2002). The crown and stem of the V3 loop play distinct roles in human immunodeficiency virus type 1 envelope glycoprotein interactions with the CCR5 coreceptor. *J. Virol.* **76**, 8953–8957.
17. Huang, C. C., Tang, M., Zhang, M. Y., Majeed, S., Montabana, E., Stanfield, R. L. *et al.* (2005). Structure of a V3-containing HIV-1 gp120 core. *Science*, **310**, 1025–1028.
18. Kondru, R., Zhang, J., Ji, C., Mirzadegan, T., Rotstein, D., Sankuratri, S. & Dioszegi, M. (2008). Molecular interactions of CCR5 with major classes of small-molecule anti-HIV CCR5 antagonists. *Mol. Pharmacol.* **73**, 789–800.
19. Dragic, T., Trkola, A., Thompson, D. A., Cormier, E. G., Kajumo, F. A., Maxwell, E. *et al.* (2000). A binding pocket for a small molecule inhibitor of HIV-1 entry within the transmembrane helices of CCR5. *Proc. Natl Acad. Sci. USA*, **97**, 5639–5644.
20. Nishikawa, M., Takashima, K., Nishi, T., Furuta, R. A., Kanzaki, N., Yamamoto, Y. & Fujisawa, J. (2005). Analysis of binding sites for the new small-molecule CCR5 antagonist TAK-220 on human CCR5. *Antimicrob. Agents Chemother.* **49**, 4708–4715.
21. Seibert, C., Ying, W., Gavrilov, S., Tsamis, F., Kuhmann, S. E., Palani, A. *et al.* (2006). Interaction of small molecule inhibitors of HIV-1 entry with CCR5. *Virology*, **349**, 41–54.
22. Maeda, K., Das, D., Ogata-Aoki, H., Nakata, H., Miyakawa, T., Tojo, Y. *et al.* (2006). Structural and molecular interactions of CCR5 inhibitors with CCR5. *J. Biol. Chem.* **281**, 12688–12698.
23. Tsamis, F., Gavrilov, S., Kajumo, F., Seibert, C., Kuhmann, S., Ketas, T. *et al.* (2003). Analysis of the mechanism by which the small-molecule CCR5 antagonists SCH-351125 and SCH-350581 inhibit human immunodeficiency virus type 1 entry. *J. Virol.* **77**, 5201–5208.
24. Nakata, H., Maeda, K., Miyakawa, T., Shibayama, S., Matsuo, M., Takaoka, Y. *et al.* (2005). Potent anti-R5 human immunodeficiency virus type 1 effects of a CCR5 antagonist, AK602/ONO4128/GW873140, in a novel human peripheral blood mononuclear cell nonobese diabetic-SCID, interleukin-2 receptor gamma-chain-knocked-out AIDS mouse model. *J. Virol.* **79**, 2087–2096.
25. Wu, L., LaRosa, G., Kassam, N., Gordon, C. J., Heath, H., Ruffing, N. *et al.* (1997). Interaction of chemokine receptor CCR5 with its ligands: multiple domains for HIV-1 gp120 binding and a single domain for chemokine binding. *J. Exp. Med.* **186**, 1373–1381.
26. Samson, M., LaRosa, G., Libert, F., Paindavoine, P., Detheux, M., Vassart, G. & Parmentier, M. (1997). The second extracellular loop of CCR5 is the major determinant of ligand specificity. *J. Biol. Chem.* **272**, 24934–24941.
27. Okada, T., Sugihara, M., Bondar, A. N., Elstner, M., Entel, P. & Buss, V. (2004). The retinal conformation and its environment in rhodopsin in light of a new 2.2 A crystal structure. *J. Mol. Biol.* **342**, 571–583.
28. Gether, U. & Kobilka, B. K. (1998). G protein-coupled receptors: II. Mechanism of agonist activation. *J. Biol. Chem.* **273**, 17979–17982.
29. Farrens, D. L., Altenbach, C., Yang, K., Hubbell, W. L. & Khorana, H. G. (1996). Requirement of rigid-body motion of transmembrane helices for light activation of rhodopsin. *Science*, **274**, 768–770.
30. Okada, T., Fujiyoshi, Y., Silow, M., Navarro, J., Landau, E. M. & Shichida, Y. (2002). Functional role of internal water molecules in rhodopsin revealed by X-ray crystallography. *Proc. Natl Acad. Sci. USA*, **99**, 5982–5987.
31. Siciliano, S. J., Kuhmann, S. E., Weng, Y., Madani, N., Springer, M. S., Lineberger, J. E. *et al.* (1999). A critical site in the core of the CCR5 chemokine receptor required for binding and infectivity of human immunodeficiency virus type 1. *J. Biol. Chem.* **274**, 1905–1913.
32. Palczewski, K., Kumasaka, T., Hori, T., Behnke, C. A., Motoshima, H., Fox, B. A. *et al.* (2000). Crystal structure of rhodopsin: a G protein-coupled receptor. *Science*, **289**, 739–745.
33. Rosenkilde, M. M. & Schwartz, T. W. (2006). GluVII:06—a highly conserved and selective anchor point for non-peptide ligands in chemokine receptors. *Curr. Top. Med. Chem.* **6**, 1319–1333.
34. Ballesteros, J. A., Jensen, A. D., Liapakis, G., Rasmussen, S. G., Shi, L., Gether, U. & Javitch, J. A. (2001). Activation of the beta 2-adrenergic receptor involves disruption of an ionic lock between the cytoplasmic ends of transmembrane segments 3 and 6. *J. Biol. Chem.* **276**, 29171–29177.
35. Olson, W. C., Rabut, G. E., Nagashima, K. A., Tran, D. N., Anselma, D. J., Monard, S. P. *et al.* (1999). Differential inhibition of human immunodeficiency virus type 1 fusion, gp120 binding, and CC-chemokine activity by monoclonal antibodies to CCR5. *J. Virol.* **73**, 4145–4155.
36. Lee, B., Sharron, M., Blanpain, C., Doranz, B. J., Vakili, J., Setoh, P. *et al.* (1999). Epitope mapping of CCR5 reveals multiple conformational states and distinct but overlapping structures involved in chemokine and coreceptor function. *J. Biol. Chem.* **274**, 9617–9626.

37. Rasmussen, S. G., Choi, H. J., Rosenbaum, D. M., Kobilka, T. S., Thian, F. S., Edwards, P. C. *et al.* (2007). Crystal structure of the human beta$_2$ adrenergic G-protein-coupled receptor. *Nature*, **450**, 383–387.
38. Sherman, W., Day, T., Jacobson, M. P., Friesner, R. A. & Farid, R. (2006). Novel procedure for modeling ligand/receptor induced fit effects. *J. Med. Chem.* **49**, 534–553.
39. Kuhmann, S. E., Pugach, P., Kunstman, K. J., Taylor, J., Stanfield, R. L., Snyder, A. *et al.* (2004). Genetic and phenotypic analyses of human immunodeficiency virus type 1 escape from a small-molecule CCR5 inhibitor. *J. Virol.* **78**, 2790–2807.
40. Trkola, A., Kuhmann, S. E., Strizki, J. M., Maxwell, E., Ketas, T., Morgan, T. *et al.* (2002). HIV-1 escape from a small molecule, CCR5-specific entry inhibitor does not involve CXCR4 use. *Proc. Natl Acad. Sci. USA*, **99**, 395–400.
41. Baba, M., Miyake, H., Wang, X., Okamoto, M. & Takashima, K. (2007). Isolation and characterization of human immunodeficiency virus type 1 resistant to the small-molecule CCR5 antagonist TAK-652. *Antimicrob. Agents Chemother.* **51**, 707–715.
42. Westby, M., Smith-Burchnell, C., Mori, J., Lewis, M., Mosley, M., Stockdale, M. *et al.* (2007). Reduced maximal inhibition in phenotypic susceptibility assays indicates that viral strains resistant to the CCR5 antagonist maraviroc utilize inhibitor-bound receptor for entry. *J. Virol.* **81**, 2359–2371.
43. Marozsan, A. J., Kuhmann, S. E., Morgan, T., Herrera, C., Rivera-Troche, E., Xu, S. *et al.* (2005). Generation and properties of a human immunodeficiency virus type 1 isolate resistant to the small molecule CCR5 inhibitor, SCH-417690 (SCH-D). *Virology*, **338**, 182–199.
44. Pugach, P., Marozsan, A. J., Ketas, T. J., Landes, E. L., Moore, J. P. & Kuhmann, S. E. (2007). HIV-1 clones resistant to a small molecule CCR5 inhibitor use the inhibitor-bound form of CCR5 for entry. *Virology*, **361**, 212–228.
45. LaBranche, C., Kitrinos, K., Howell, R., McDanal, C., Harris, S., Jeffrey, J. & Demarest, J. (2005). Targeting HIV Entry, 1st International Workshop, Bethesda, MD, December 2–3, Abstract 9.
46. Nishizawa, R., Nishiyama, T., Hisaichi, K., Matsunaga, N., Minamoto, C., Habashita, H. *et al.* (2007). Spirodiketopiperazine-based CCR5 antagonists: lead optimization from biologically active metabolite. *Bioorg. Med. Chem. Lett.* **17**, 727–731.
47. Kimpton, J. & Emerman, M. (1992). Detection of replication-competent and pseudotyped human immunodeficiency virus with a sensitive cell line on the basis of activation of an integrated beta-galactosidase gene. *J. Virol.* **66**, 2232–2239.
48. Maeda, Y., Foda, M., Matsushita, S. & Harada, S. (2000). Involvement of both the V2 and V3 regions of the CCR5-tropic human immunodeficiency virus type 1 envelope in reduced sensitivity to macrophage inflammatory protein 1alpha. *J. Virol.* **74**, 1787–1793.
49. Gartner, S., Markovits, P., Markovitz, D. M., Kaplan, M. H., Gallo, R. C. & Popovic, M. (1986). The role of mononuclear phagocytes in HTLV-III/LAV infection. *Science*, **233**, 215–219.
50. Koyanagi, Y., O'Brien, W. A., Zhao, J. Q., Golde, D. W., Gasson, J. C. & Chen, I. S. (1988). Cytokines alter production of HIV-1 from primary mononuclear phagocytes. *Science*, **241**, 1673–1675.
51. Jacobson, M. P., Pincus, D. L., Rapp, C. S., Day, T. J., Honig, B., Shaw, D. E. & Friesner, R. A. (2004). A hierarchical approach to all-atom protein loop prediction. *Proteins*, **55**, 351–367.
52. Xiang, Z. & Honig, B. (2001). Extending the accuracy limits of prediction for side-chain conformations. *J. Mol. Biol.* **311**, 421–430.
53. Kaminski, G. A., Friesner, R. A., Tirado-Rives, J. & Jorgensen, W. J. (2001). Evaluation and reparameterization of the OPLS-AA force field for proteins via comparison with accurate quantum chemical calculations on peptides. *J. Phys. Chem. B*, **105**, 6474–6487.
54. Still, W. C., Tempczyk, A., Hawley, R. C. & Hendrickson, T. (1990). Semianalytical treatment of solvation for molecular mechanics and dynamics. *J. Am. Chem. Soc.* **112**, 6127–6129.
55. Friesner, R. A., Banks, J. L., Murphy, R. B., Halgren, T. A., Klicic, J. J., Mainz, D. T. *et al.* (2004). Glide: a new approach for rapid, accurate docking and scoring: 1. Method and assessment of docking accuracy. *J. Med. Chem.* **47**, 1739–1749.
56. Friesner, R. A., Murphy, R. B., Repasky, M. P., Frye, L. L., Greenwood, J. R., Halgren, T. A. *et al.* (2006). Extra precision Glide: docking and scoring incorporating a model of hydrophobic enclosure for protein–ligand complexes. *J. Med. Chem.* **49**, 6177–6196.
57. Jeeninga, R. E., Hoogenkamp, M., Armand-Ugon, M., de Baar, M., Verhoef, K. & Berkhout, B. (2000). Functional differences between the long terminal repeat transcriptional promoters of human immunodeficiency virus type 1 subtypes A through G. *J. Virol.* **74**, 3740–3751.

Erythromycin derivatives inhibit HIV-1 replication in macrophages through modulation of MAPK activity to induce small isoforms of C/EBPβ

Iwao Komuro*†, Toshiaki Sunazuka‡, Kiyoko S. Akagawa*‡, Yasuko Yokota*, Aikichi Iwamoto†, and Satoshi Ōmura‡§

*Department of Immunology, National Institute of Infectious Diseases, 1-23-1 Toyama, Shinjuku-ku, Tokyo 162-8640, Japan; †Division of Infectious Diseases, Advanced Clinical Research Center, Institute of Medical Science, University of Tokyo, 4-6-1 Shiroganedai, Minato-ku, Tokyo 108-8639, Japan; and ‡Kitasato Institute for Life Sciences, Kitasato University and the Kitasato Institute, 5-9-1 Shirokane, Minato-ku, Tokyo 108-8641, Japan

Contributed by Satoshi Ōmura, June 18, 2008 (sent for review January 11, 2008)

Macrophages (MΦs) are a major source of HIV-1 especially in patients with tuberculosis. There are MΦs that are permissive and those that restrict HIV-1. Regulation of hematopoietic cell kinase (Hck) activity and selective expression of CCAAT enhancer binding protein β (C/EBPβ) isoforms greatly contribute to determine distinct susceptibility of MΦs to HIV-1. Resistance is attributable to reduced expression of Hck and augmented expression of an inhibitory small isoform of C/EBPβ. Derivatives of erythromycin A (EMA) EM201 and EM703 inhibit the replication of HIV-1 in tissue MΦs, at posttranscriptional and translational levels. We demonstrate that EM201 and EM703 convert tissue MΦs from HIV-1 susceptible to HIV-1 resistant through down-regulation of Hck and induction of small isoforms of C/EBPβ. These drugs inhibit p38MAPK activation which is expressed only in susceptible tissue MΦs. Activated CD4⁺T cells stimulate the viral replication in HIV-1 resistant MΦs through down-regulation of small isoforms of C/EBPβ via activation of ERK1/2. EM201 and EM703 can inhibit the MAPK activation and inhibit the burst of viral replication produced when CD4⁺T cells and MΦs interact. These EM derivatives may be highly beneficial for repression of residual HIV-1 in the lymphoreticular system of HIV-1-infected patients and offer great promise for the creation of new anti-HIV drugs for the future treatment of AIDS patients.

AIDS | macrolides | Hck

At least 65 million people have been infected with HIV and AIDS has killed 25 million people since 1981. By 2007, worldwide, 39.5 million individuals were living with HIV, with 4.3 million new infections and 2.9 million deaths occurring in 2006 (http://data.unaids.org/pub/EpiReport/2006/02-Global_Summary_2006_EpiUpdate_eng.pdf). In developed countries, anti-HIV-1 therapy—highly active antiretroviral therapy (HAART)— potently inhibits HIV-1 replication, reduces viral antigenemia, and prolongs the survival of patients (1, 2). In contrast, patients in developing countries generally cannot use HAART therapy because of its high cost and the sheer number of patients. Furthermore, HAART therapy cannot remove HIV-1-infected latent memory T cells and monocytes (Mos)/macrophages (MΦs) in some lymphoreticular tissue, residual cells having the potential to become a viral resource capable of spreading new viral particles (3, 4). Therefore, the development of new drugs to improve and extend HAART therapy, particularly in countries in the developing world, is greatly and urgently needed.

Mos/MΦs are a major target of HIV-1 infection and serve as a reservoir for viral persistence and a chronic source of infectious virus *in vivo* (5). Most tissue MΦs are permissive to M-tropic virus entry and release a small number of virus particles in the asymptomatic carrier but they occasionally produce a large number of viral particles in the AIDS patients or HIV-1 patients with pulmonary tuberculosis (TB) or those whose conditions are complicated with opportunistic infection (3). TB markedly increases HIV-1 replication and mutation in the lung and is associated with an acceleration of AIDS (6, 7). The alveolar MΦ is the major cell type in which HIV-1 replication occurs during TB (8, 9). Thus MΦ is a key factor in the control of HIV-1 suffering.

We and others have previously demonstrated that expression of tyrosine kinase hematopoietic cell kinase (Hck) and relative amounts of a large isoform (37-kDa) to a small isoform (23-kDa) (L/S ratio) of transcription factor CCAAT enhancer binding protein β (C/EBPβ) play critical roles in M-tropic HIV-1 production in tissue MΦs (8, 10–13). We have also reported that modulation of the expression of Hck and the L/S ratio of C/EBPβ by treatment with antisense oligonucleotides can convert the phenotype of HIV-1 suceptibility in MΦs (10). These studies suggest that, not only anti-HIV-1 drugs that directly affect the virus (such as RT inhibitor or protease inhibitors), but also drugs that can convert the phenotype of tissue MΦs from "susceptible" to "resistant" by down-regulating the expression of Hck and enhancing the expression of small isoforms of C/EBPβ may be useful to help control HIV-1 replication in AIDS patients.

Macrolides with a 14-membered ring structure, such as erythromycin A (EMA), clarithromycin (CAM), or roxithromycin (RXM), are well known antibacterial drugs. Recently, these antibiotics have been shown to be efficacious against incurable chronic inflammatory airway disease, such as diffuse panbronchiolitis (DPB) (14, 15). This therapeutic efficacy is thought to be caused by either anti-inflammatory or immunomodulatory activity of the macrolide antibiotics, which can act on many cells, including epithelial cells, neutrophiles, monocytes/MΦs, and T cells (16–23). On the basis of this knowledge, we chemically modified EMA to obtain derivatives with both stronger capability for promoting monocyte-to-MΦ differentiation and no antibacterial activity. Among the derivatives, 8,9-anhydroerythromycin A 6,9-hemiketal (EM201), obtained by mild acid treatment of EMA, already known as an internal metabolite of EMA, showed a strong promotional effect on MΦ differentiation and possessed weak antimicrobial activity (24). Furthermore, the 12-membered pseudoerythromycin A (EM703) was both remarkably active and free of any antibacterial activity (25) and was known to exhibit a prophylactic effect on lung injury *in vivo* against a bleomycin-induced acute lung injury in the rat model, similar to EMA (26).

In this study, we show that both EM201 and EM703 are good lead candidates for drugs that can inhibit M-tropic HIV-1 replication in tissue MΦs by a new way of converting their phenotype from HIV-1-susceptible to HIV-1-resistant, through down-regulation of Hck and the induction of small isoforms of C/EBPβ via modulation of the activation of MAPKs.

Author contributions: T.S., K.S.A., and S.Ō. designed research; I.K., T.S., and K.S.A. performed research; T.S., Y.Y., and S.Ō. contributed new reagents/analytic tools; I.K., T.S., K.S.A., A.I., and S.Ō. analyzed data; and I.K., T.S., K.S.A., and S.Ō. wrote the paper.

The authors declare no conflict of interest.

§To whom correspondence should be addressed. E-mail: omuras@insti.kitasato-u.ac.jp.

This article contains supporting information online at www.pnas.org/cgi/content/full/0805504105/DCSupplemental.

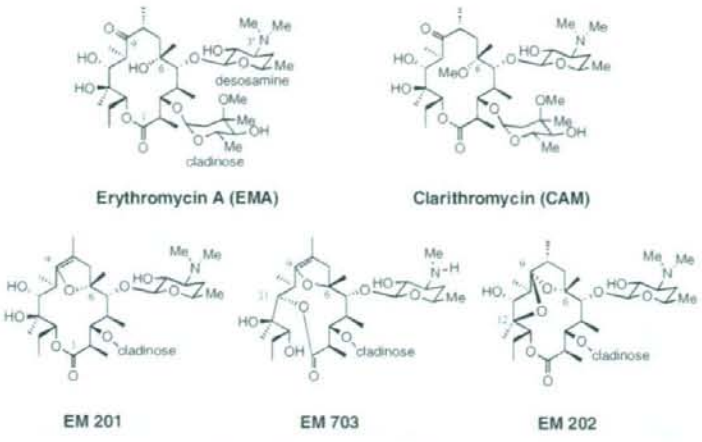

Fig. 1. Structure of EM derivatives.

Results

Effects of EM Derivatives on Viral Replication and Multinucleated Giant Cell Formation in M-Tropic HIV-1-Infected M-MΦs. We first examined whether EM derivatives (Fig. 1) have an ability to inhibit M-tropic HIV-1 replication in macrophage colony-stimulating factor (M-CSF)-induced monocyte-derived MΦs (M-MΦs), which express a high level of Hck and a large isoform of C/EBPβ, are susceptible to M-tropic HIV-1 replication, and whether they form multinucleated giant cells (MGC) by cell-to-cell fusion at 4–7 d after infection (10, 27). EM201 and EM703 (30 μM) completely inhibited viral replication and MGC formation at 7 d after infection, while EMA, CAM, and EM202 did not (Fig. 2*A*). PCR using a primer pair designed from the HIV-1 LTR region of HIV-1_{BaL} DNA at 2 d after infection showed that the DNA replication at first replicon was observed at similar levels in all of the M-MΦs. At 7 d after infection, however, the levels of viral DNA in M-MΦs treated with EMA, EM202, or DMSO (solvent) alone increased, whereas those in M-MΦs treated with EM201and EM703 remained low, at levels similar to those observed at 2 d after infection (Fig. 2*A*).

EM201 and EM703 (30 μM) persistently inhibited viral replication at 14 d (Fig. 2*B*), and inhibition was observed even at 21 d after infection (data not shown). EM201 and EM703 strongly inhibited HIV-1_{BaL} replication, even at 3 μM, and p24 levels were ~4% of those in cells treated with DMSO alone at 14 d after infection (Fig. 2*C*). EMA and EM202 induced inhibition of viral replication at higher concentration (>300 μM). However, the reduction curves in cells were similar to those in DMSO-treated cells (Fig. 2*C*), indicating the effects are mainly because of DMSO toxicity. In contrast, CAM partially but significantly inhibited HIV-1_{Bal} replication at 10–30 μM at 10 and 14 d after infection (Figs. 2 *B* and *C*), and it is impossible to deny that CAM itself can inhibit HIV-1 replication.

EM201 and EM703 Modulate the Expression of Hck and C/EBPβ Proteins in HIV-1_{BaL} Infected M-MΦs. To examine the possibility that EM201 and EM703 inhibit HIV-1 replication in M-MΦs via modulation of the expression of Hck and C/EBPβ, expression of these proteins in HIV-1 infected M-MΦs treated with 30 μM EM derivatives was examined by immunoblots at 2 d after infection. The levels of Hck protein in M-MΦs treated with EM201 and EM703 strongly decreased to one-seventh and one-ninth of that in M-MΦs treated with DMSO alone, respectively (Fig. 3*A*). Conversely, the small isoform of C/EBPβ protein was strongly induced in M-MΦs treated with EM201 and EM703, the levels increasing to 25- to 40-fold of that in M-MΦs treated with DMSO alone, with the L/S ratio of C/EBPβ markedly decreasing from 12.6 to 0.3 and 0.5, respectively (Fig. 3*A*).

EMA and EM202 did not affect the expression of Hck and C/EBPβ and consequently did not inhibit viral replication (Fig. 3*A*). Similarly CAM, which did not show inhibitory activity during the early phase of infection, did not significantly affect expression of either Hck or C/EBPβ at 2 d after infection.

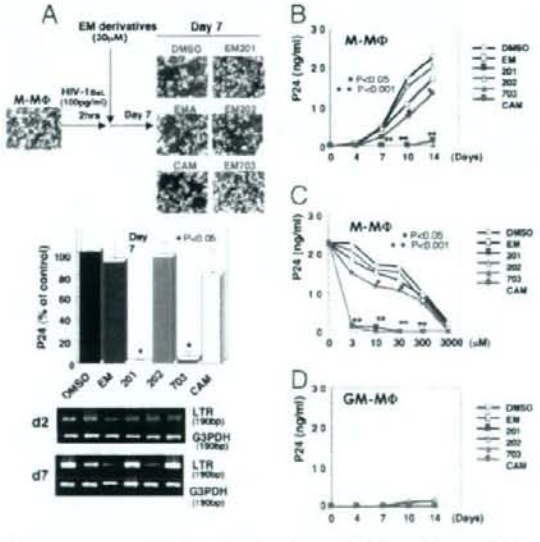

Fig. 2. Screening of EM derivatives that show an inhibitory effect on HIV-1_{BaL} replication in M-MΦs. (*A*) Effects of 30 μM of EMA (EM), CAM, EM201 (201), EM202 (202), and EM703 (703) on viral replication and MGC formation (Magnification, 100) at 7 d after infection. The data of viral production were shown as the percentage of p24 antigen in control (DMSO alone) M-MΦs. The levels of viral DNA were assayed at 2 and 7 d after infection. (*B*) Kinetics of viral production in HIV-1 infected M-MΦs treated with 30 μM of EM derivatives. (*C*) Dose-response effects of EM derivatives on HIV-1 replication in M-MΦs at 14 d after infection. (*D*) EM derivatives (30 μM) do not change the resistant phenotype against HIV-1 infection in GM-MΦs. The data shown are representative one of five independent experiments.

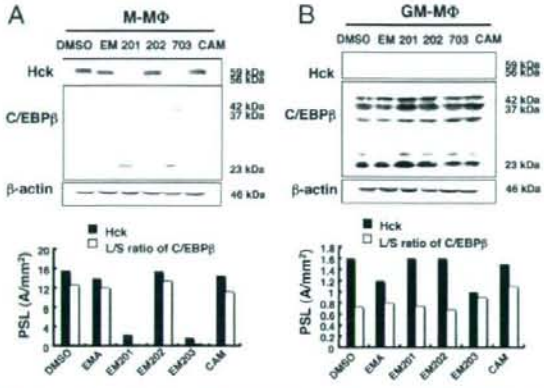

Fig. 3. Effects of EM derivatives on the expression of Hck and C/EBPβ in HIV-1_{BaL}-infected M-MΦs and GM-MΦs. Immunoblots of Hck and C/EBPβ in M-MΦs (*A*) and GM-MΦs (*B*) at 2 d after infection. EMA (EM), EM201 (201), EM202 (202), EM703 (703), and CAM were added at 30 μM. The relative amounts of Hck and C/EBPβ were measured using National Institutes of Health image software (PSL; photo stimulating luminescence, A/mm²). The relative amounts of the large band to the small band (L/S ratio) of C/EBPβ were calculated using PSL values of 37 kDa and 23 kDa of C/EBPβ isoforms and are shown at the bottom of each figure. The data shown are representative of one of three independent experiments.

EM201 and EM703 Change Neither the Expression of Hck and C/EBPβ Proteins Nor the Resistant Phenotype Against HIV-1 Infection in GM-MΦs. Granulocyte-macrophage CSF (GM-CSF)-induced monocyte-derived MΦ (GM-MΦ) is HIV-1 resistant and does not stimulate the replication of M-tropic HIV-1and MGC formation. This is because GM-MΦs express a high level of short isoforms of C/EBPβ and a low level of Hck, and HIV-1 infection drastically increases the expression of a short isoform of C/EBPβ but decreases that of Hck (10). We examined the effects of EM derivatives on viral replication and the expression of Hck and C/EBPβ in HIV-1_{BaL}-infected GM-MΦs. Even at 14 d after infection, we found that GM-MΦs treated with various kinds of EM derivatives (including EM201 and EM703) did not stimulate viral replication (Fig. 2*D*) or MGC formation (data not shown). Consistent with the lack of change in HIV-1 resistant phenotype, all of the EM derivatives did not affect the expression of Hck and C/EBPβ protein in GM-MΦs (Fig. 3*B*).

p38MAPK Inhibitor, but Not ERK1/2 Inhibitor, Inhibits Viral Replication in M-Tropic HIV-1 Infected M-MΦs via Reduced Expression of Hck and Increased Expression of a Small Isoform of C/EBPβ. Previous reports have shown that the replication of M-tropic HIV-1 in tissue MΦs requires the activation of p38MAPK (28) and that ERK1/2 mediates the activation of C/EBPβ (29, 30). We consequently examined the activation of MAPKs in HIV-1 susceptible M-MΦs and HIV-1 resistant GM-MΦs. Expressions of total and phosphorylated forms of p38MAPK in M-MΦs were higher than those in GM-MΦs before HIV-1_{BaL} infection (Fig. 4*A*). After infection, the phosphorylated form was augmented in M-MΦs but not in GM-MΦs (Fig. 4*A*). In contrast to p38MAPK, the expressions of total and phosphorylated forms of ERK1/2 in M-MΦs were lower than those in GM-MΦs before infection, but the expression was unchanged in both MΦs after infection (Fig. 4*A*). Consistent with the augumented activation of p38MAPK in M-MΦs, addition of p38MAPK inhibitor SB203580 (at 10 μM) completely suppressed viral replication and MGC formation in HIV-1_{BaL}-infected M-MΦs (Fig. 4*B*).

We subsequently investigated whether the inhibitory activity of SB203580 on viral replication in HIV-1_{BaL}-infected M-MΦs is mediated through modulation of the expression of Hck and C/EBPβ protein. SB203580 not only inhibited the phosphorylation of p38MAPK but also reduced the expression of Hck and increased the expression of the small isoform of C/EBPβ to mimic the inhibitory effect on viral replication (Fig. 4 *C–E*). Conversely, the ERK1/2 inhibitor PD98059 affected neither viral replication nor the expression of Hck and C/EBPβ protein (Fig. 4 *B–E*).

EM201 and EM703 Inhibit Viral Replication in M-Tropic HIV-1 Infected M-MΦs via Inhibition of p38MAPK Activation. The above results suggest that EM201 and EM703 inhibit M-tropic HIV-1 replication

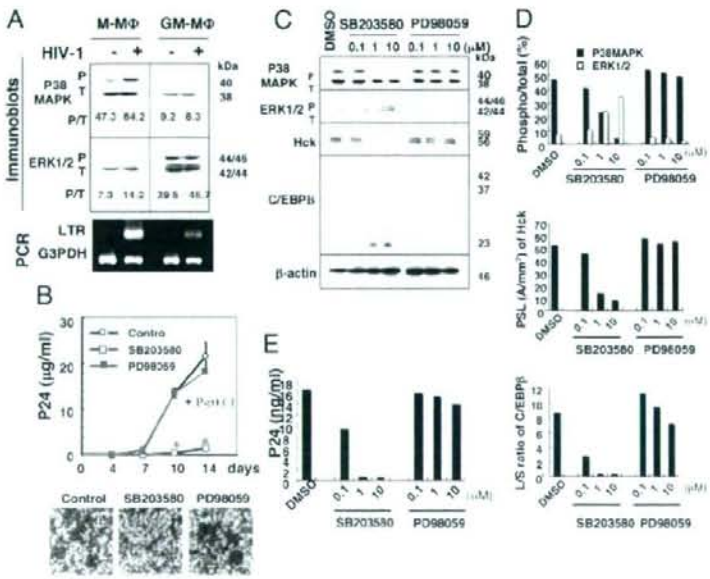

Fig. 4. Effects of p38 MAPK inhibitor and ERK1/2 inhibitor on viral replication and expression of Hck and C/EBPβ in HIV-1_{BaL}infected M-MΦs. (*A*) Immunoblot analysis of total and phosphorylated forms of p38MAPK and ERK1/2 in M-MΦs and GM-MΦs before and 2 d after infection. (*B*) Kinetic analysis of viral replication and morphology in HIV-1_{BaL}-infected M-MΦs treated with 10 μM of SB203580 or PD98059. (*C*) Immunoblot analysis of Hck and C/EBPβ in HIV-1_{BaL}-infected M-MΦs treated with various concentrations of SB203580 or PD98059 at 2 d after infection. (*D*) The relative amounts of Hck and L/S ratio of C/EBPβ in the cells or the phosphorylated protein *P* to the total protein *T* (P/T ratio) of p38 MAPK and ERK1/2 in immunoblot analysis shown in *c* calculated as described in Fig. 3. (*E*) Viral production in HIV-1_{BaL}-infected M-MΦs treated with various concentrations of SB203580 or PD98059. The data shown are representative of one of three independent experiments.

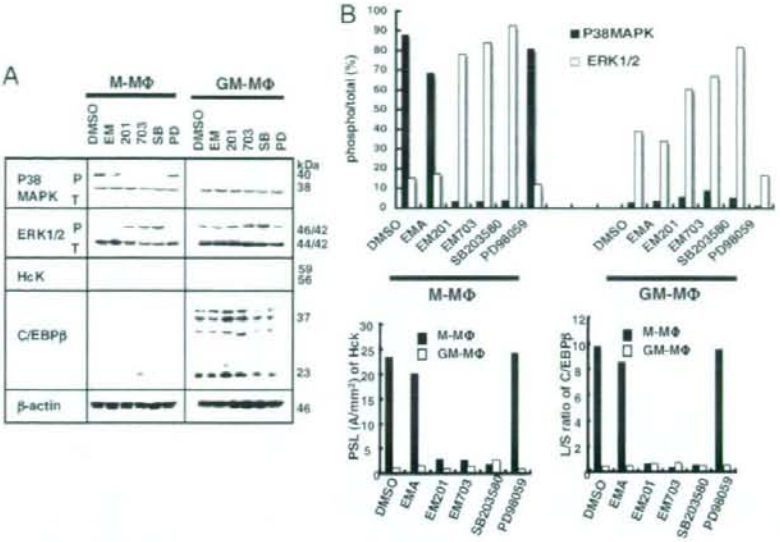

Fig. 5. Effects of EM derivatives on the phosphorylation of p38 MAPK and ERK1/2 in M-MΦs and GM-MΦs. (*A*) Immunoblot analysis of Hck and C/EBPβ, and the phosphorylation of p38 MAPK and ERK1/2 in M-MΦs and GM-MΦs treated with 30 μM of EMA (EM), EM201 (201), EM703 (703), 10 μM of SB203580 (SB), or PD98059 (PD), and DMSO alone at 2 d after HIV-1 infection. (*B*) The relative amounts of Hck and L/S ratio of C/EBPβ or P/T ratio of p38 MAPK and ERK1/2 in immunoblot analysis shown in *a* are calculated as described in Fig. 3. The data shown are representative of one of three independent experiments.

via inhibition of p38MAPK activation. To help confirm this hypothesis, we examined the effect of EM201 or EM703 (30 μM) on the phosphorylation of p38MAPK and ERK1/2 in M-MΦs by immunoblot. EM201 and EM703, but not EMA, reduced phosphorylation of p38MAPK but enhanced the phosphorylation of ERK1/2 in HIV-1-infected M-MΦs at 2 d after treatment (Fig. 5).

As described above, EM201 and EM703 did not affect the HIV-1-resistant phenotype of GM-MΦs (Figs. 2*D* and 3*B*). Consistent with the results, none of the EM derivatives significantly affected the phosphorylation pattern of p38MAPK and ERK1/2 in HIV-1-infected GM-MΦs (Fig. 5).

Activated CD4⁺T Cells Stimulate Viral Replication in M-Tropic HIV-1 Infected GM-MΦs via Down-Regulation of a Small Isoform of C/EBPβ. Recently, Hosino *et al.* (9) reported a phenotypical change of human alveolar MΦs (A-MΦs) from resistant to susceptible for HIV-1 replication caused by the addition of activated lymphocytes. The change was brought about by decreased expression of a small isoform of C/EBPβ (9). In line with this report, the addition of activated CD4⁺T cells to HIV-1_{BaL}-infected GM-MΦs stimulated marked viral replication (Fig. 6*A*), with MGC formation and clusters of GM-MΦs with CD4⁺ T cells (data not shown) at 10–14 d after infection. The amounts of viral DNA in the GM-MΦs increased at 2–7 d after infection (Fig. 6*B*). In GM-MΦs stimulated with activated CD4⁺ T cells, expression of the small isoform of C/EBPβ protein significantly decreased whereas the L/S ratio of C/EBPβ increased (from 0.57 to 3.6) at 2 d after infection (Fig. 6 *C* and *D*). Expression of Hck in the GM-MΦs, however, did not change significantly, even after stimulation with activated T cells and was very low compared with that in M-MΦs (Fig. 6 *C* and *D*).

Activated CD4⁺T Cells Down-Regulate the Small Isoform of C/EBPβ in M-Tropic HIV-1-Infected GM-MΦs via Augmentation of ERK1/2 Phosphorylation. As described above, activation of p38MAPK but not ERK1/2 is critical for HIV-1 replication in M-MΦs. However, the p38MAPK inhibitor, SB203580, did not inhibit viral replication in GM-MΦs stimulated with activated CD4⁺T cells (Fig. 6*A*). Instead, the ERK1/2 inhibitor PD98059 completely inhibited viral replication (Fig. 6*A*) and suppressed the level of viral DNA to that observed in the culture of GM-MΦs alone in which viral replication was absent (Fig. 6*B*). Upon examination of the phosphorylation of p38MAPK and ERK1/2 in HIV-1_{BaL}-infected GM-MΦs stimulated with activated CD4⁺ T cells, the phosphorylation ratio of ERK1/2 but not of p38MAPK significantly increased in GM-MΦs stimulated with activated CD4⁺ T cells, compared with that in GM-MΦs alone. Addition of PD98059 not only inhibited the phosphorylation of ERK1/2 but also increased expression of the small isoform of C/EBPβ, while markedly decreasing the L/S ratio of C/EBPβ from 3.6 to 0.82 (Fig. 6 *C* and *D*). The addition of SB203580 did not affect the expression of C/EBPβ. The expression of Hck was unaffected by treatment with either of the two inhibitors (Fig. 6 *C* and *D*).

EM201 and EM703 Inhibit M-Tropic HIV-1 Replication in GM-MΦs Stimulated with Activated CD4⁺ T Cells via Inhibition of the Activation of ERK1/2 and Augmentation of the Expression of the Small Isoform of C/EBPβ. In examining whether EM201 and EM703 can inhibit viral replication in M-tropic HIV-1-infected GM-MΦs stimulated with activated CD4⁺T cells, addition of EM201 and EM703 (30 μM) completely inhibited viral replication (Fig. 6*A*) and MGC formation (data not shown). The levels of HIV-1 DNA observed were very low, the same as those seen in the culture of GM-MΦs alone (Fig. 6*B*).

We subsequently examined the effects of EM201 and EM703 on the expression of Hck and C/EBPβ and on the phosphorylation of p38MAPK and ERK1/2 in HIV-1_{BaL}-infected GM-MΦs stimulated with activated CD4⁺ T cells at 2 d after infection by immunoblot. Treatment with EM201 and EM703 did not change the levels of Hck protein, but increased levels of the small isoform of C/EBPβ protein and the L/S ratio of C/EBPβ decreased from 3.6 to 0.45 (EM201) and 0.44 (EM703) (Fig. 6 *C* and *D*). The phosphorylation level of ERK1/2 decreased following treatment with EM201 and EM703, but that of p38MAPK remained unchanged (Fig. 6 *C* and *E*).

Discussion

In this study, we demonstrated that two EMA derivatives, EM201and EM703, can inhibit the replication of M-tropic HIV-1 in tissue MΦs at the posttranscriptional and translational levels, but do not affect viral entry and first DNA replicon. The inhibition is

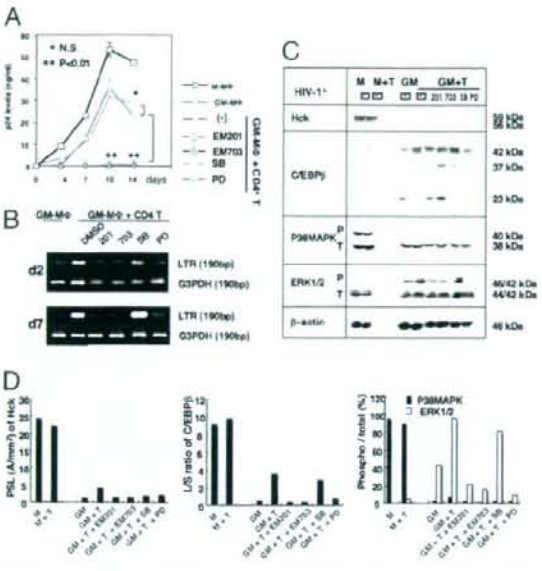

Fig. 6. Augmentation of M-tropic HIV-1 production in GM-MΦs stimulated with CD4$^+$ T cells, and the suppressive effects of EM201 and EM703 on viral replication through the induction of small isoforms of C/EBPβ via inhibition of phosphorylation of ERK1/2. M-MΦs and GM-MΦs were infected with HIV-1_{BaL}. Part of HIV-1-infected GM-MΦs were stimulated with activated CD4$^+$ T cells and incubated with or without 30 μM of EMA (EM), EM201 (201), or EM703 (703), 10 μM of SB203580 (SB), or PD98059 (PD), and DMSO alone. (*A*) Kinetic analysis of HIV-1 replication. (*B*) Levels of viral DNA at 2 and 7 d after infection. (*C*) Immunoblot analysis of Hck, C/EBPβ, and phosphorylation of p38 MAPK and ERK1/2 at 2 d after infection. (*D*) The relative amounts of Hck and L/S ratio of C/EBPβ or P/T ratio of p38 MAPK and ERK1/2 in immunoblot analysis shown in *c* calculated as described in Fig. 3. (*M*) M-MΦ; GM, GM-MΦ; T, T cells; 201, EM201; 703, EM703; SB, SB203580; and PD, PD98059. The data shown are representative of one of three independent experiments.

caused by a new means of converting the phenotype of tissue MΦs, from HIV-1 susceptible to HIV-1 resistant, via down-regulation of Hck and induction of the small isoform of C/EBPβ through modulation of the activation of MAPKs. Consistent with the previous report (9), we showed that HIV-1-resistant GM-MΦs, require stimulation with activated CD4$^+$ T cells to produce vigorous virus production. This is mediated by down-regulation of the expression of the small isoform of C/EBPβ. Both EM201 and EM703 potently inhibit viral replication, not only in M-MΦs but also in GM-MΦs stimulated with activated CD4$^+$ T cells via inhibiting the down-regulation of the expression of the small isoform of C/EBPβ.

Both EM201 and EM703 change the phenotype only of HIV-1-susceptible MΦs. They do not affect the phenotype of HIV-1-resistant GM-MΦs. HIV-1 susceptibility and the expression of Hck and C/EBPβ proteins in A-MΦs from normal healthy volunteers are the same as those in GM-MΦs (8, 10). Therefore EM201 and EM703 do not change the resistant phenotype of A-MΦs. This would be beneficial for healthy A-MΦs in the HIV-1 carrier, by maintaining resistance against HIV-1 replication.

In the present study, we demonstrated that activation of p38MAPK and ERK1/2 play a critical role in HIV-1 production via down-regulation of the small isoform of C/EBPβ in HIV-1-infected-M-MΦs and -GM-MΦs stimulated with activated CD4$^+$ T cells, respectively. This study shows that different MAPKs play crucial roles in HIV-1 production in different types of tissue MΦs. P38MAPK activation in HIV-1-infected M-MΦs link to the augmented expression of Hck and the maintenance of the low level of the small isoform of C/EBPβ. We previously reported that reduced expression of Hck in M-MΦs with antisense oligonucleotide for Hck stimulates the induction of the short isoform of C/EBPβ and inhibits the viral replication (10). Our present results, taken together with the previous study, show the unique evidence that the p38MAPK signal cascade is upstream of Hck expression and is linked to down-regulation of the small isoform of C/EBPβ in HIV-1-susceptible M-MΦs. However, ERK1/2-mediated down-regulation of the small isoform of C/EBPβ in HIV-1-infected GM-MΦs stimulated with activated CD4$^+$ T cells does not link to Hck expression.

Interestingly, EM201 and EM703, in contrast to existing MAPK inhibitors, can inhibit viral replication via prevention of the activation of respective MAPKs in both HIV-1-infected-M-MΦs and -GM-MΦs stimulated with activated T cells, where different MAPKs play a critical role for viral replication. Such a novel and unique suppressive mechanism of EM201 and EM703 on HIV-1 replication in tissue MΦs may be useful for the future treatment of AIDS patient.

The anti-HIV-1 activity of EM201 and EM703 does not relate to their antibiotic activity, because they have only weak (EM201) or completely lack (EM703) such antibiotic activity (24, 25). At present, we do not know what kind of structure activity relationships exist in EM201 and EM703. Recently, calmodulin- and calmodulin-dependent protein kinase-II (CaMK-II)-dependent activation of p38MAPK has been reported in HIV accessory protein, Tat-induced IL-10 expression in normal human monocytes (31). EM201 and EM703 are known to act as inhibitors of intracellular Ca^{2+} level and Ca^{2+} oscillation (21, 32, 33). These characteristics may contribute to the novel anti-HIV-1 mechanism of EM201 and EM703.

Macrolides, such as EMA and CAM, are known to be specifically accumulated into tissue MΦs and stay stable at high levels for long periods because of a low rate of breakdown and excretion (34). EM201 and EM703 potently inhibit HIV-1 replication in MΦs at low levels, such as 30 μM, that correspond to the concentration of EMA or CAM in MΦs after oral intake of EMA, 400 mg or CAM 200 mg/day (usual doses are 1600 mg and 400 mg/day, respectively). Furthermore, inhibition of viral replication can be observed at lower concentrations, such as 3 μM, which is sustained for 2–14 days after infection. These findings offer advantages with respect to drug specificity and reduction of drug toxicity. In addition, these new macrolides are derived from EMA (24, 25) and would be very inexpensive. Thus, these substances offer great potential for the creation of new anti-HIV-1 drugs for the future treatment of AIDS patients.

Materials and Methods

Erythromycin Derivatives. EMA was purchased from Sigma-Aldrich. CAM was supplied by Taisho Pharmaceutical. EM201, EM202, and EM703 were prepared as described previously (24, 25).

Preparation and Culture of MΦs. Monocytes (Mos) and Mo-derived Mp were prepared as described previously (10, 35). M-CSF-induced monocyte-derived MΦs and GM-CSF-induced monocyte-derived MΦs were called M-MΦs and GM-MΦs, respectively. [see supporting information (SI) *Materials and Methods* for a detailed description].

HIV-1 Strain and Infection. M-tropic HIV-1 strain, HIV-1_{BaL}, was collected from culture supernatant of the HIV-1 strain-infected M-MΦs as a viral resource. Mo-derived MΦs were incubated for 2 h at 37°C with 100 pg/ml p24 antigen of DNase-treated viral supernatant (p24, the 50% tissue culture infective dose ($TCID_{50}$) and multiplicity of infection (MOI) are 50 ng/ml, ~3,000 and 0.05, respectively) and then cultured in RPMI MEDIUM 1640 containing 10% FCS and CSF. If necessary, the viral inoculum was pretreated with 100 μM AZT for 2 h at 4°C (5). Fresh culture medium containing CSF was added every 3–4 d (20% of the volume). Heat-inactivated virus (1 h, 56°C) was used as negative control. Viral production was assayed by sequential measurement of p24 antigen in superna-

tants by an ELISA using a combination of two antibodies; anti-gag-p24 monoclonal antibody (Nu24) and peroxidase-labeled 1085 (36), or the RETRO-TEK HIV-1 p24 antigen ELISA kit for high-affinity detection of low levels of p24 antigen (ZeptoMetrix, Buffalo, New York).

Coculture of HIV-1 Infected GM-MΦs with the Activated CD4$^+$T Cells. CD4$^+$ T cells were positively isolated from CD14$^-$ PBMCs using a MACS with anti-CD4 mAb coated microbeads. The selected population was >93% positive for CD3 and CD4. Activated CD4$^+$ T cells were prepared by stimulation with PHA and cultured with IL-2 (30 unit/ml) (Genzyme). GM-MΦs were incubated for 2 h at 37°C with 100 pg/ml p24 antigen of DNase-treated viral supernatant, washed twice, and then cocultured with the activated CD4$^+$ T cells in the presence of IL-2.

Detection of HIV-1 DNA by Nested PCR. Detection of HIV-1 DNA by nested PCR was performed as described previoiusly (10). HIV LTR and gag primers were JAM 62 and JAM 65. For the nested PCR, JAM 63 and JAM 64 were used as internal primers (36). (see *SI Materials and Methods* for a detailed description).

Immunblot Analysis. Immunoblot analysis was performed as described in ref. 10. Antibodies against the following proteins were used: rabbit polyclonal antibody against Hck (N-30), C/EBPβ (C-19) (Santa Cruz Biotechnology), phospho-specific (Tyr 182) p38 mitogen-activated protein kinase (P38MAPK) (no. 9211), p38 MAPK (no. 9212), phospho-specific (Tyr 204) phosphorylated extracellular signal-regulated kinases (ERK)1/2 (no. 9101), ERK1/2 antibody (no. 9102) (New England BioLabs), or normal rabbit IgG. Horseradish peroxidase-conjugated goat anti-rabbit IfG (sx-2030)(Santa Cruz Biotechnology) was used as secondary Ab. The blots were visualized with Amersham ECL Reagent on Hyper ECL-film (Amersham). (see *SI Materials and Methods* for a detailed description).

Statistical Analysis. Statistical analysis of the data were performed using Student's *t test*. *P*-values <0.01 were considered significant. The experiments shown are representatives of three to seven independent experiments.

ACKNOWLEDGMENTS. This work was supported in part by grants for Research on Health Sciences Focusing on Drug Innovation from the Japan Health Sciences Foundation and the Ministry of Health, Labor and Welfare of Japan.

1. Cavert W, *et al.* (1997) Kinetics of response in lymphoid tissues to antiretroviral therapy of HIV-1 infection. *Science* 276:960–964.
2. Perelson AS, *et al.* (1997) Decay characteristics of HIV-1-infected compartments during combination therapy. *Nature* 387:188–191.
3. Orenstein JM, Fox C, Wahl SM (1997) Macrophages as a source of HIV during opportunistic infections. *Science* 276:1857–1861.
4. Crowe SM, Sonza S (2000) HIV-1 can be recovered from a variety of cells including peripheral blood monocytes of patients receiving highly active antiretroviral therapy: A further obstacle to eradication. *J Leukoc Biol* 68:345–350.
5. Orenstein JM (2001) The macrophage in HIV infection. *Immunobiol* 204:598–602.
6. Nakata K, *et al.* (1997) Mycobacterium tuberculosis enhances human immunodeficiency virus-1 replication in the lung. *Am J Resp Crit Care Med* 155:996–1003.
7. Whalen C, *et al.* (1995) Accelerated course of human immunodeficiency virus infection after tuberculosis. *Am J Respir Crit Care Med* 151:129–135.
8. Honda Y, *et al.* (1998) Type I interferon induces inhibitory 16-kD CCAAT/enhancer binding protein (C/EBP)beta, repressing the HIV-1 long terminal repeat in macrophages: Pulmonary tuberculosis alters C/EBP expression, enhancing HIV-1 replication. *J Exp Med* 188:1255–1265.
9. Hoshino Y, *et al.* (2002) Maximal HIV-1 replication in alveolar macrophages during tuberculosis requires both lymphocyte contact and cytokines. *J Exp Med* 195:495–505.
10. Komuro I, Yokota Y, Yasuda S, Iwamoto A, Akagawa KS (2003) CSF-induced and HIV-1-mediated distinct regulation of Hck and C/EBPbeta represent a heterogeneous susceptibility of monocyte-derived macrophages to M-tropic HIV-1 infection. *J Exp Med* 198:443–453.
11. Henderson AJ, Calame KL (1997) CCAAT/enhancer binding protein (C/EBP) sites are required for HIV-1 replication in primary macrophages but not CD4(+) T cells. *Proc Natl Acad Sci USA* 94:8714–8719.
12. Weiden M, *et al.* (2000) Differentiation of monocytes to macrophages switches the mycobacterium tuberculosis effect on HIV-1 replication from stimulation to inhibition: Modulation of interferon response and CCAAT/enhancer binding protein beta expression Type I interferon induces inhibitory 16-kD CCAAT/enhancer binding protein (C/EBP)beta, repressing the HIV-1 long terminal repeat in macrophages: Pulmonary tuberculosis alters C/EBP expression, enhancing HIV-1 replication. *J Immunol* 165:2028–2039.
13. Hogan TH, Krebs FC, Wigdahl B (2002) Regulation of human immunodeficiency virus type 1 gene expression and pathogenesis by CCAAT/enhancer binding proteins in cells of the monocyte/macrophage lineage. *J Neurovirol* 8 Suppl 2:21–26.
14. Kudoh S, Uetake K, Hagiwara K (1987) Clinical effect of low dose long term erythromycin chemotherapy on diffuse panbronchiolitis. *Jap J Thorac Dis* 25:632–642.
15. Kadota J, *et al.* (1993) A mechanism of erythromycin treatment in patients with diffuse panbronchiolitis. *Am Rev Respir Dis* 147:153–159.
16. Sugawara E (1997) Effect of macrolide antibiotics on neutrophil function in human peripheral blood. *Kansenshogaku Zasshi* 71:329–336.
17. Sunazuka T, *et al.* (1999) Effects of erythromycin and its derivatives on Interleukin-8 release by human bronchial epithelial cell line BEAS-2B cells. *J Antibiot* 52:71–74.
18. Oohori M, *et al.* (2000) Effect of 14-membered ring macrolide compounds on rat leucocytes chemotaxis and the structure-activity relationships. *J Antibiot* 53:1219–1222.
19. Keicho N, Kudoh S, Yotsumoto H, Akagawa KS (1993) Erythromycin promotes monocytes to macrophage differentiation. *J Antibiot* 47:80–89.
20. Keicho N, Kudoh S, Yotsumoto H, Akagawa KS (1993) Antilymphocytic activity of erythromycin distinct from that of FK506 or cyclosporin A. *J Antibiot* 46:1406–1413.
21. Kudoh S, *et al.* (2002) Novel activity of erythromycin and its derivatives. *Macrolide Antibiotics, Chemistry, Biology, and Practice*, eds Omura S (Academic), 2nd Ed, pp 533–569.
22. Culic O, Erakovic V, Parnham MJ (2001) Anti-inflammatory effects of macrolide antibiotics. *Eur J Pharmacol* 429:209–229.
23. Labro MT (2001) Anti-inflammatory activity of macrolides: A new therapeutic potential? *J Antimicrob Chemother* 41(Suppl B):37–46.
24. Sunazuka T, *et al.* (2003) Effect of 14-membered macrolide compounds on monocyte to macrophage differentiation. *J Antibiot* 5:721–724.
25. Yoshida K, *et al.* (2005) Macrolides with promotive activity of monocyte to macrophage differentiation. *J Antibiot* 58:79–81.
26. Ying JL, *et al.* (2006) EM703 improves bleomycin-induced pulmonary fibrosis in mice by the inhibition of TGF-beta signaling in lung fibroblasts. *Respir Res* 7:16:1–13.
27. Matsuda S, *et al.* (1995) Suppression of HIV replication in human monocyte-derived macrophages induced by granulocyte/macrophage colony-stimulating factor. *AIDS Res Hum Retroviruses* 11:1031–1038.
28. Muthumani K, *et al.* (2004) Suppression of HIV-1 viral replication and cellular pathogenesis by a novel p38/JNK kinase inhibitor. *Aids* 18:739–748.
29. Nakajima T, *et al.* (1993) Phosphorylation at threonine-235 by a ras-dependent mitogen-activated protein kinase cascade is essential for transcription factor NF-IL6. *Proc Natl Acad Sci USA* 90:2207–2211.
30. Giltiay NV, Karakashian AA, Alimov AP, Ligthle S, Nikolova-Karakashian MN (2005) Ceramide- and ERK-dependent pathway for the activation of CCAAT/enhancer binding protein by interleukin-1beta in hepatocytes. *J Lipid Res* 46:2497–2505.
31. Gee K, Angel JB, Mishra S, Blahoianu MA, Kumar A (2007) IL-10 regulation by HIV-Tat in primary human monocytic cells: Involvement of calmodulin/calmodulin-dependent protein kinase-activated p38 MAPK and Sp-1 and CREB-1 transcription factors. *J Immunol* 178:798–807.
32. Sunazuka T, Omura S (2004) Creation of a new macrolide derivative, EM703. *Jpn J Antibiot* 57(Suppl A):114–116.
33. Hattori R, Shimizu T, Shimizu S, Majima Y (2004) Effect of EM703, a new macrolide derivative, on mucus secretion from the airway epithelial cells. *Jpn J Antibiot* 57(Suppl A):123–125.
34. Fietta A, Merlini C, Gialdroni GG (1997) Requirements for intracellular accumulation and release of clarithromycin and azithromycin by human phagocytes. *J chemotherapy* 9:23–31.
35. Akagawa KS (2002) Functional heterogeneity of colony-stimulating factor induced human monocyte-derived macrophages. *Int J Hematol* 76:27–34.
36. Tsunetsugu-Yokota Y, *et al.* (1995) Monocyte-derived cultured dendritic cells are susceptible to human immunodeficiency virus infection and transmit virus to resting T cells in the process of nominal antigen presentation. *J Virol* 69:4544–4547.

ELSEVIER

INSTITUT PASTEUR

Microbes and Infection 11 (2009) 191–197

www.elsevier.com/locate/micinf

Original article

Activation of HIV-1 Gag-specific CD8$^+$ T cells by yeast-derived VLP-pulsed dendritic cells is influenced by the level of mannose on the VLP antigen

Fuminori Mizukoshi [a], Takuya Yamamoto [a], Yu-ya Mitsuki [a], Kazutaka Terahara [a], Ai Kawana-Tachikawa [b], Kazuo Kobayashi [a], Aikichi Iwamoto [b], Yuko Morikawa [c], Yasuko Tsunetsugu-Yokota [a,*]

[a] *Department of Immunology, National Institute of Infectious Diseases, Toyama 1-23-1 Shinjuku-ku, Tokyo, Japan*
[b] *Department of Infectious Diseases, Institute of Medical Science, University of Tokyo, Shirokanedai 4-6-1, Minato-ku, Tokyo, Japan*
[c] *Kitasato Institute for Life Sciences and Graduate School for Infection Control, Kitasato University, Shirokane 5-9-1, Minato-ku, Tokyo, Japan*

Received 3 October 2008; accepted 12 November 2008
Available online 24 November 2008

Abstract

Dendritic cells (DCs) are professional antigen-presenting cells that possess a unique capacity to cross-present exogenous antigens efficiently to CD8$^+$ T cells. We previously demonstrated that monocyte-derived DCs (MDDCs) pulsed with yeast-derived HIV-1 Gag virus-like particles (VLPs) were able to activate Gag-specific CD8$^+$ T cells from HIV-1-infected individuals. Yeast VLPs are abundantly mannosylated (high-mannose type: HmVLPs) and are highly immunogenic. Because lectin receptors are shown to negatively regulate Th1 responses, we investigated the relationship between VLP mannosylation level and MDDC cross-presentation activity. Poorly mannosylated VLPs (low-mannose type: LmVLPs) were prepared using a yeast mnn9 mutant strain that lacks a core mannosylation enzyme. We found that MDDCs pulsed with LmVLPs activated Gag-specific T cells more strongly than those pulsed with HmVLPs. However, MDDCs showed similar antigen uptake and intracellular transport of both types of VLPs. Interestingly, LmVLPs induced IL-12 production slightly more than HmVLPs (yet statistically significant). Furthermore, the level of LPS-induced IL-10 production was enhanced by pulsing with HmVLPs, but not with LmVLPs. These results indicate that lectin receptors recognizing mannose may influence the Th1/Th2 balance of the immune response, resulting in reduced efficiency of CD8$^+$ T cell activation by a heavily mannosylated antigen presented by DCs.

Keywords: Antigen presentation; Mannosylation; AIDS

1. Introduction

Dendritic cells (DCs) are professional antigen-presenting cells that play a pivotal role in the immune system by acting as "sentinel cells" [1]. DC-based immunotherapy has been developed to treat a variety of diseases, including cancer [2,3], autoimmune diseases [4], transplant rejection [5], allergic diseases [6], and infectious diseases [7]. Previous studies of human immunodeficiency virus (HIV) and simian immunodeficiency virus (SIV) infections demonstrated that monocyte-derived DCs (MDDCs) pulsed with inactivated viruses enhanced both cellular and humoral immune responses [8,9]. However, the efficacies of DC-based immunotherapy for clinical applications have been inconsistent, probably because of the different protocols for cultivating and maturating the DCs, for the selection and loading of antigens, and for the administration, route, dose, and frequency of the therapy.

* Corresponding author: Tel.: +81 3 5285 1111x2133; fax: +81 3 5285 1150 or 1156.
E-mail address: yyokota@nih.go.jp (Y. Tsunetsugu-Yokota).

1286-4579/$ - see front matter Crown Copyright © 2008 Published by Elsevier Masson SAS. All rights reserved.
doi:10.1016/j.micinf.2008.11.004

Acquired immune deficiency syndrome (AIDS), which is caused by HIV infection, is an enormous public health threat worldwide. The development of highly active anti-retroviral therapy (HAART) has markedly improved treatment of HIV-infected individuals and has significantly reduced HIV-associated mortality [10]. However, HAART cannot completely eradicate HIV [11]. Therefore, a novel strategy is required for treating HIV infections.

In terms of the host immune response against HIV, antigen-specific $CD8^+$ cytotoxic T lymphocytes (CTLs) are known to be important in suppressing HIV replication [12]. Therefore, CTL-inducible vaccines have been developed, most of them virus-based [13]. We previously showed that DCs pulsed with yeast-derived HIV-1 Gag virus-like particles (VLPs) activated Gag-specific T cells *in vitro* [14]. Because VLPs are neither infectious nor replicative, and also can be easily produced on a large scale, a VLP-based vaccine is an excellent candidate for a vaccine based on cross-presentation.

Highly glycosylated antigens have strong immunogenicity, whether expressed by yeast or using a baculoviral system. For example, mannosylation of antigens augments antigen-specific T cell responses [15,16]. However, recent studies revealed that the stimulation of lectin receptors on DCs induced interleukin (IL)-10 production, resulting in a shift in immune regulation towards Th2 dominance [17–19]. Thus, the influence of carbohydrate chains on the immune response is a concern for novel vaccine developments.

We postulated that the cross-presentation activity of DC is influenced by the degree of antigen mannosylation. In this study, we compared the antigenicity of abundantly mannosylated VLPs derived from a wild-type yeast to that of poorly mannosylated VLPs derived from a yeast mnn9 mutant lacking mannosylating enzyme.

2. Materials and methods

2.1. Preparation of cells

Fresh peripheral blood mononuclear cells (PBMCs) were obtained from healthy donors by Ficoll density gradient centrifugation. $CD14^+$ cells were positively isolated from PBMCs using a MACS system (Miltenyi Biotech, Bergisch Gladbach, Germany) according to the manufacturer's protocol. We generated immature MDDCs using 10 ng/ml human granulocyte-macrophage colony-stimulating factor and 20 ng/ml IL-4 as previously described [14]. These blood samples were collected with written informed consent under the approval of the ethical committee in National Institute of Infectious Diseases (NIID).

A Gag28 peptide (p17:KYKLKHIVW)-specific CTL line was established from PBMCs of HIV-1-infected individuals carrying HLA-A*2402 as previously described [20]. The studies utilizing PBMCs of HIV-infected patients were approved by the ethical committees in NIID and the Institute of Medical Science (University of Tokyo), and PBMCs were collected with written informed consent.

2.2. Production and purification of yeast-derived HIV-1 Gag VLPs

Wild-type yeast-derived VLPs from HIV-1 Gag, VLPs fused with green fluorescent protein (EGFP) and control culture supernatant (CS) were produced as described previously [14,21]. The mutant *S. cerevisiae* mnn9 strain [22] was used to produce low mannose-type VLPs. Standard purification and sucrose density gradient analysis of Gag VLPs was performed as described previously [23]. Purified VLPs were obtained by fractionation of the gradients. For comparison, *Spodoptera frugiperda* (*Sf*9) cells were infected with recombinant *Autographa californica* nuclear polyhedrosis viruses (baculoviruses) containing the full-length HIV-1 *gag* gene [23]. Purified Gag VLPs were quantitated by Coomassie brilliant blue staining. Total yeast protein was quantified by Bradford's method [21].

2.3. Quantitative analysis of mannose on the VLPs with dot blot technique

The samples were diluted with PBS and applied to a nitrocellulose membrane (0.45 μm pore size; GE Osmonics Labstore, Minnetonka, MA) using BioDot SF microfiltration apparatus (BioRad, Hercules, CA) according to the manufacturer's instructions. The membrane was soaked three times in blocking buffer (10 mM Tris–HCl pH 7.4, 0.15 M NaCl, 0.05% Tween20) for 10 min at room temperature (RT), then reacted with the biotinylated ConA (EY Laboratories, Inc., San Mateo, CA) (10 μg/ml in blocking buffer) for 90 min. After washing three times with blocking buffer, the membrane was incubated for 30 min at RT with horseradish peroxidase (HRP)-conjugated streptavidin (Boehringer-Roche, Basel, Switzerland) (1:5000 dilution). The SuperSignal West Dura kit (Pierce, Rockford, IL) was used for detection and the signal was analyzed by LAS-3000 (Fujifilm, Tokyo, Japan). The luminescence intensity of each dot was measured using Image Gauge densitometry software (version 4.0; Fujifilm).

2.4. Endocytosis assay

Immature MDDCs were incubated with various concentrations of CS or high- or low-mannose type VLP-EGFP at 37 °C for 3 h. These cells were washed extensively with flow cytometry (FCM) buffer (2% v/v fetal bovine serum and 50 μg/ml sodium azide in PBS), and resuspended in FCM buffer containing propidium iodide. The uptake of VLP-EGFP was quantified by measuring the fluorescence intensity using FACScalibur and CellQuest software (Becton Dickinson, Labware, NJ). For the receptor blocking assay, immature MDDCs were pre-cultured for 30 min in the presence of mAb against dendritic cell-specific intracellular adhesion molecule-3-grabbing nonintegrin (DC-SIGN) (10 μg/ml; eBioscience, San Diego, CA), mannose receptor (MR) mAb (10 μg/ml; BD Bioscience, Flanklin Lakes, NJ), mannan (2 mg/ml; Sigma–Aldrich) or isotype control IgG_{2a} (10 μg/ml; eBioscience), then pulsed with VLPs (10 μg/ml) or fluorescein-isothiocyanate

(FITC)-conjugated mannosylated BSA (man-BSA; Sigma–Aldrich) (100 μg/ml).

2.5. Subcellular fractionation and Western blotting analysis

Immature MDDCs cultured with 40 μg/ml of high- or low-mannose type VLPs were washed with PBS and then fractionated into cytosol and membrane/organelle fractions using ProteoExtract subcellular proteome extraction kit (Calbiochem, Darmstadt, Germany).

For Western blotting, cells or subcellular fractions were resuspended in lysis buffer (10 mM Tris–HCl pH 7.4, 150 mM NaCl, 1% sodium deoxycholate, 1% Triton X-100, 0.1% sodium dodecyl sulfate, 357.5 mM 2-mercaptoethanol). The lysate, containing 2×10^5 cells, was analyzed by 12.5% SDS-PAGE and electrophoretically transferred to a PVDF transfer membrane (Amersham Biosciences, Buckinghamshire, UK). Non-specific binding was blocked with washing buffer (10 mM Tris–HCl, 150 mM NaCl, 0.05% Tween 20) containing 3% skim milk for 30 min at RT. After washing, the membrane was stained for 1 h at RT either with the anti-Calpain mAb (Calbiochem) as a cytosolic marker or anti-gastrin-releasing peptide (GRP) 78 mAb (BD Bioscience) as a membrane/organelle marker. Subsequently, the membrane was incubated with biotin-conjugated anti-mouse IgG for 1 h at RT, followed by streptavidin-conjugated HRP (Boehringer-Roche) for 30 min at RT. Gag p24 was detected by incubation with HRP-conjugated anti-HIV Gag mAbs (clone 10B5; kindly provided by T. Sata, Department of Pathology, NIID, Tokyo, Japan) [24] for 1 h at RT. The immunoreactive bands were detected with SuperSignal West Dura kit and visualized by Lumino analyzer LAS-3000.

2.6. Detection of cytokines

To detect IFN-γ production, an enzyme-linked immunospot (ELISPOT) assay was carried out as previously described [14]. The culture supernatant was collected and the level of cytokines was measured with the cytometric beads array kit (BD Bioscience) according to the manufacturer's protocol.

3. Results

3.1. Characterization of VLPs generated from yeast mutant mnn9

To determine whether the level of antigen mannosylation can modulate the immune response, we generated VLPs from wild-type yeast and from the mannosyltransferase mutant mnn9. The mnn mutants are mostly defective in polymerization enzymes related to the synthesis of the outer chain portion of N-linked oligosaccharides, and the mnn9 strain is defective in the core enzyme for glycosylation [25]. The wild-type yeast-derived VLPs are heavily mannosylated and are designated as high-mannose type VLPs (HmVLPs); in contrast, mnn9 mutants produce poorly mannosylated VLPs (low-mannose type VLPs: LmVLPs). The mannosylation level of LmVLPs is considered to be more similar to the level of mannose on mammalian mannoproteins than that of HmVLPs.

Using sucrose density gradient analysis, HmVLPs were recovered mainly at the density of 1.210 g/ml (Fig. 1A, upper panel), while the major peak density of LmVLPs was at 1.196 g/ml (Fig. 1A, middle panel) and the major peak of baculovirus-based VLPs was at 1.180 g/ml (Fig. 1A, lower panel). Thus, the LmVLPs are smaller in size than HmVLPs, probably due to the lower degree of mannosylation.

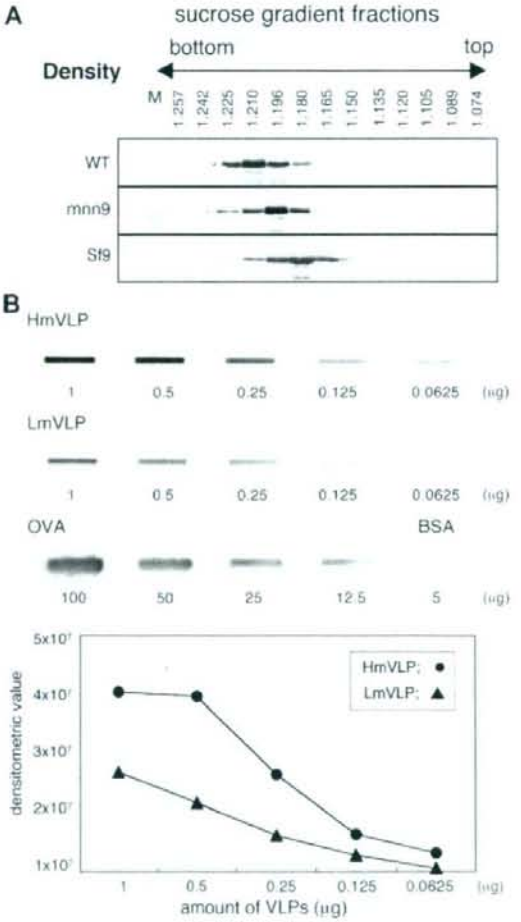

Fig. 1. Characterization of yeast VLPs. (A) Sucrose density gradient fractions were analyzed by Western blotting using anti-Gag mAbs. (Upper panel) HmVLPs derived from wild-type *S. cerevisiae* (WT). (Middle panel) LmVLPs derived from mnn9 mutant strain (mnn9). (Lower panel) VLPs derived from Sf9. 40 μg of VLPs were applied per assay, respectively. (B) Lectin staining was carried out on using biotinylated ConA and HRP-conjugated avidin. The number is indicative of the volume of sample applied per slot. The densitometric value of HmVLPs (filled circle) or LmVLPs (filled triangle) was measured by the computerization.

We next estimated the level of the mannosylation on these VLPs using lectin blot. In comparison with the LmVLPs generated from the mnn9 mutants, HmVLPs generated from a wild-type yeast strain clearly showed higher levels of mannose (Fig. 1B). As control, no mannose was detected in native BSA, while OVA was highly mannosylated. These results indicate that LmVLPs and HmVLPs differ in their mannose glycosylation levels.

3.2. The effect of uptake and intracellular dynamics of HmVLPs and LmVLPs

We first studied the internalization efficiency of EGFP-fused VLPs by MDDCs. We titrated the uptake of these VLPs at various concentrations (5–20 μg/ml). Both VLPs were taken up by MDDCs in a dose-dependent manner (Fig. 2A, upper panels), although the uptake of HmVLP was slightly better than that of LmVLP at 5 μg/ml.

In order to understand the mechanism of uptake of these VLPs by MDDCs, we carried out the blocking experiment. The uptake of these HmVLP and LmVLP at 10 μg/ml was strongly inhibited by mannan, but neither by anti-MR nor by anti-DC-SIGN mAbs (Fig. 2A, lowest panels). In contrast, the uptake of a high dose of man-BSA was remarkably inhibited by the same concentration of anti-MR, but not by anti-DC-SIGN mAb. Therefore, MDDCs are able to take up these VLPs at a similar level, probably by the mannose-mediated mechanism, but neither via DC-SIGN nor MR.

For cross-presentation of VLPs, the antigens incorporated in MDDCs have to be transported into the cytosol and processed by the proteasomes. To test whether the intracellular transport of VLPs is influenced by their level of mannosylation, the MDDCs were pulsed for 1 or 6 h with the

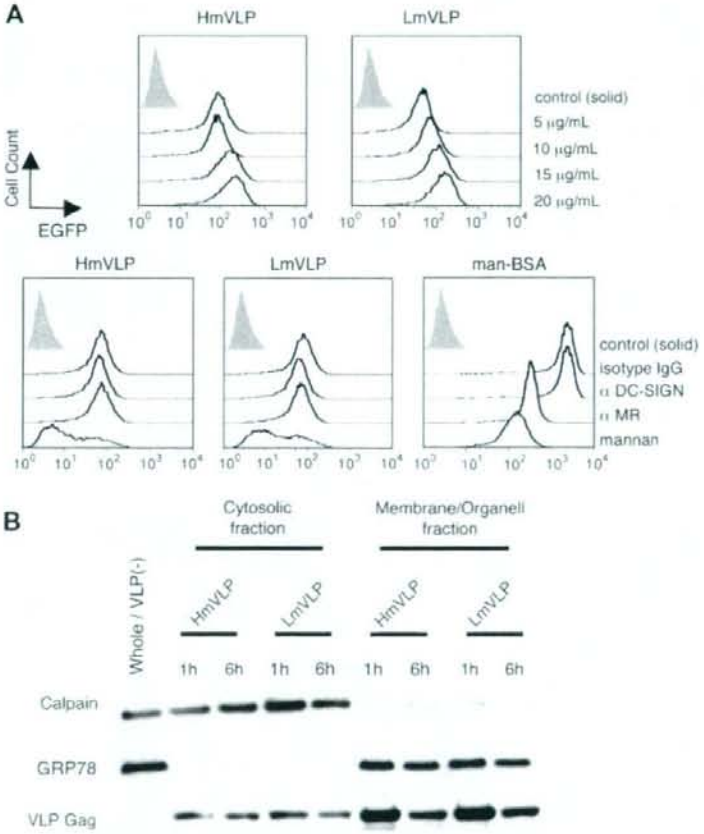

Fig. 2. Uptake and localization of yeast VLPs by DCs. (A) Immature MDDCs (5×10^4 cells/50 μl) were incubated with HmVLP-EGFP or LmVLP-EGFP (upper panel, indicated concentrations; lower panel, 10 μg/ml) for 3 h, analyzed by flow cytometry. Moreover, MDDCs were pre-incubated for 30 min with indicated antibodies (10 μg/ml) or mannan (2 mg/ml), and pulsed with HmVLP-EGFP or LmVLP-EGFP (10 μg/ml), mannosylated BSA (100 μg/ml) as a control (lower panel). The background signal is shown as a shadow. (B) Immature MDDCs (1×10^6 cells/200 μl) were incubated with 40 μg/ml yeast HmVLPs, LmVLPs or CS for 1 or 6 h, and fractionated. Whole cell lysate [Whole/VLP(−)] and cytosolic and membrane/organelle fractions were analyzed by Western blotting using antibodies against the cytosolic marker Calpain, the membrane marker GFP78, and VLP Gag.

VLPs at a high concentration (40 μg/ml) to obtain a strong signal, and fractionated. The level of HIV-1 Gag protein in the cytosolic and membrane/organelle fractions was analyzed by Western blot (Fig. 2B). As control, the calpain was detected mainly on the cytosolic fraction, whereas GRP78 was detected exclusively on the membrane/organelle fraction. There was no clear difference in the amount of Gag protein present in the cytosolic fractions in MDDCs pulsed with HmVLPs versus LmVLPs, as well as in the membrane/organelle fraction. We concluded that the mannosylation level of VLPs does not affect the internalization or the intracellular amount of Gag antigens in MDDCs.

3.3. LmVLPs are more efficiently cross-presented than HmVLPs for CD8$^+$ T cell (CTLs) activation by MDDCs

We next tested the efficiency of these VLPs on CTL activation by MDDC-mediated cross-presentation. We utilized HIV-1 Gag28 peptide-specific CTL lines established from HLA-A24$^+$ HIV-infected patients as an indicator cell for cross-presentation efficiency. Frozen HLA-A24$^+$ healthy donor-derived MDDCs were pulsed either with 10 μg/ml of HmVLPs or LmVLPs, cocultured with Gag-specific CTL lines for 40 h, and analyzed by IFN-γ ELISPOT.

For this experiment, three independent CTL lines (CTL #9, #21, and #31) were cocultured with VLP-pulsed MDDCs derived from two donors each (Fig. 3). Despite the MDDCs' donor variation, LmVLP-pulsed MDDCs were able to activate higher numbers of Gag28-specific CTL lines compared to HmVLP-pulsed MDDCs in four of six MDDCs. Thus, our results suggest that the level of mannose on antigens can modulate the cross-presenting activity of VLPs by MDDCs.

3.4. Cytokine production by MDDCs after uptake of VLPs is influenced by the level of VLP mannosylation

For effective induction of CTL activity, it is important to polarize DCs toward Th1-type cytokine secretion during the DC–T cell interaction. We previously showed that MDDCs stimulated with yeast VLPs produced a higher level of IL-12 than those stimulated with LPS, while IL-10 production is limited [14]. We therefore measured cytokine production by 10 μg/ml of HmVLP- or LmVLP-pulsed MDDCs from eight healthy donors. Two patterns of IL-12 production were identified: IL-12 responders ($n = 4$), and IL-12 non-responders ($n = 4$) (Fig. 4).

In the case of the IL-12 responders, IL-12 production induced by LmVLPs tended to be higher than that by HmVLP (Fig. 4A), though the difference was not statistically significant. In contrast, the level of IL-10 production was very low in these donors (data not shown).

In IL-12 non-responders, both IL-12 and IL-10 production by LmVLP- or HmVLP-pulsed MDDCs were consistently low (data not shown). When we stimulated the MDDCs from these donors with LPS, the production of IL-10, but not IL-12, was increased, and the LPS-induced IL-10 production

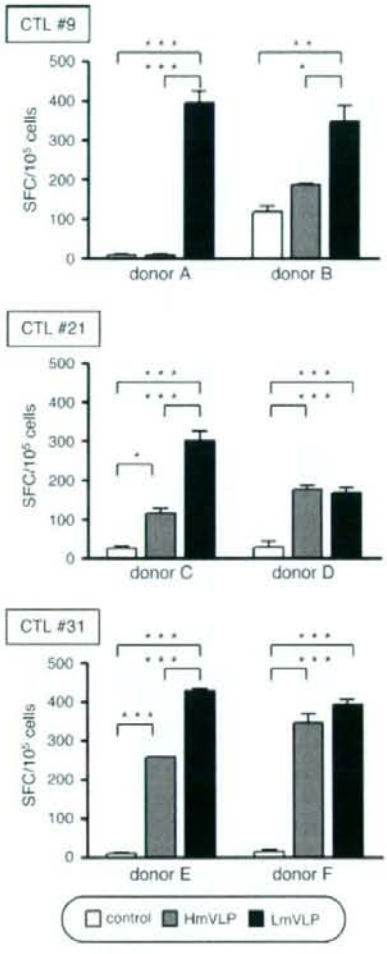

Fig. 3. The influence of yeast VLPs on HIV Gag-specific CD8$^+$ T cell activation. Immature MDDCs were pulsed overnight with 10 μg/ml HmVLPs (gray bar), LmVLPs (filled bar), or CS (open bar). Next day, MDDCs (1×10^4 cells per well) were mixed with MHC class I-matched allogenic CTL clones ($1–2 \times 10^4$ per well). Two days after cocultivation, the number of IFN-γ-producing cells was determined by ELISPOT analysis. The longitudinal axis shows the analysis spot forming cells (SFC) producing IFN-γ per 10^5 cells. Results are presented as the means + SEM. *$P < 0.05$; **$P < 0.01$; ***$P < 0.001$, compared between two groups; one-way ANOVA followed by Bonferroni's t-test ($n = 3$).

was upregulated further in the presence of HmVLPs, while it was not true for LmVLPs (Fig. 4B). The level of IL-12 production remained undetectable or low even after stimulation with LPS plus HmVLPs or LPS plus LmVLPs (data not shown). The production of other cytokines (including IL-1, IL-6, IL-8, and TNF-alpha) was very low or showed little difference in response to HmVLPs and LmVLPs. These results suggest that a high level of mannosylation modulates the cytokine production by MDDCs toward a Th2-type response.